Simultaneous Inversion of Permeability and Porosity via Collocated Cokriging

Z. A. Reza (zreza@ualberta.ca)
Department of Civil & Environmental Engineering, University of Alberta

X.H. Wen (xwen@chevrontexaco.com)
ChevronTexaco Exploration and Production Technology Company

C. V. Deutsch (cdeutsch@civil.ualberta.ca)
Department of Civil & Environmental Engineering, University of Alberta

Abstract

Optimal reservoir management requires reliable reservoir performance forecasts with as little uncertainty as possible. Incomplete data and inability to model the physics of fluid flow at a suitably small scale lead to uncertainty. Subsurface reservoir models that "by construction" honor historical production data should yield significantly more accurate predictions of reservoir performance with reduced uncertainty than those that do not. This research aims to develop a new technique that link temporal production data and static spatial constraints on the distribution of permeability and porosity in reservoir models.

The technique developed here for simultaneous inversion of permeability and porosity builds upon the approach of Sequential Self-Calibration (SSC) method for simple permeability inversion. In order to integrate both porosity and permeability simultaneously the algorithm for sensitivity coefficients of reservoir response variables with respect to reservoir parameters are modified. The algorithm relies on collocated cokriging equation for permeability models using porosity models. This paper presents the developed inversion algorithm. Applications of the algorithm to some synthetic and realistic examples have been discussed. Also discussed are a number of implementation issues and some important sensitivity studies.

Introduction

Reservoir development planning using detailed 3D reservoir models requires models of structure, stratigraphy, and properties. Interpretive, deterministic and geostatistical techniques for constructing models of lithofacies and properties are used that constrain the models to static data from core, logs, seismic, and geologic interpretation. In general, however, honoring all data including the dynamic pressure or historical production data is quite difficult. In practice, trial-and-error history matching is still the most common approach at the final stage of modeling. The problem of fully integrating production and pressure data in the construction of reservoir models lends itself to a variety of approaches. Property models within the volume of influence of a well are generated through a one-step mathematical inversion of the pressure response. The problems with these techniques are the intense computations required to generate a solution that is not unique and may be inconsistent with some of the static data. In other approaches, the property models are generated in several steps with a first-step coding of the well-derived data into a spatial property representation.

There is a strong need for improvement in the available techniques of dynamic data integration to construct realistic reservoir models. State-of-the-art technologies suffer from the limitation of not accommodating realistically complex heterogeneities of the subsurface reservoir system. Incorporation of simplistic physics and homogenization of critical reservoir features are still the only way to

resolve this reservoir characterization problem. The reason for adapting such naive approaches is not the lack of motivation, but the problem is an inverse problem and highly underdetermined.

In this paper, we present an inversion algorithm developed to simultaneously generate porosity and permeability models using available production data and static information. Applications of the algorithm to some synthetic and realistic examples have been discussed. Also discussed are a number of implementation issues and some important sensitivity studies.

Problem Description

Characterization of detailed 3-D reservoir models entails working in an almost infinite dimensional space with multitude of parameters to be estimated. There are various reservoir model properties for which inversion techniques are applied. In most cases, these reservoir parameters are communication between strata and across faults through transmissibility, distance to boundaries, effective flow capacities in the vicinity of wells, productivity of wells, measures of interwell communication (absolute/relative kh), coarse grid representation of kh, or ϕ, facies connectivity between wells, drainage volumes around wells, facies proportions around/between wells, connectivity between wells and connected surfaces,local measures of heterogeneity (e.g., variogram, covariance, mean and variance of permeability and porosity), etc.

Production data integration in reservoir characterization is an inverse problem. The intent of such study is to build numerical reservoir models that by construction integrate all types of dynamic data along with all static information about the reservoirs. In this study, an algorithm for simultaneous inversion of porosity and permeability using production data and other available static information has been developed.

Simultaneous Inversion Problem

Algorithm for simultaneous inversion of porosity and permeability is based on geostatistical techniques [2] involved in reservoir model building through static data integration. It is quite popular to build geostatistical reservoir porosity models by kriging [1] and then generate permeability models by collocated cokriging [3] method using porosity values. Thus, the inversion algorithm adopted is based on the underlying geostatistical equations.

The approach is to first do simple (or ordinary) kriging from porosity (ϕ) data to get estimation of ϕ at all locations, then perform collocated cokriging to estimate $y = \log(k)$. The simple kriging equation for ϕ at location i is

$$\phi_i = \sum_{j=1}^{n_{mp}} \tau_{i,j}^{\phi} \phi_j \tag{1}$$

where $\phi_j,\ j = 1, \ldots, n_{mp}$ are the porosity values at the master points, n_{mp} number of master points, and $\tau_{i,j}^{\phi}$ the kriging weights at a location i for porosity value at any master point ϕ_j. While the collocated cokriging equations for y_i at location i is give by

$$y_i = \sum_{j=1}^{n_{mp}} \tau_{i,j}^{y} y_j + \xi_i \phi_i \tag{2}$$

where $y_j,\ j = 1, \ldots, n_{mp}$ are the permeability logarithm values at the master points, $\tau_{i,j}^{y}$ the kriging weights at location i for y_j value at any master point, ξ_i the collocated kriging weights at location i for the collocated secondary variable ϕ_i.

Markov assumption of first kind is then used in collocated cokriging, which entails the linear regression model between y and ϕ:

$$y = \rho\phi + r \tag{3}$$

where ρ is the global correlation coefficient between y and ϕ, and r a random component.

Relationship (3) is used as a closure. Combining above relationships, we have:

$$\frac{\partial y_i}{\partial y_j} = \tau^y_{i,j} + \xi_i \frac{\partial \phi_i}{\partial y_j} = \tau^y_{i,j} + \xi_i \frac{\partial \phi_i}{\partial \phi_j}\frac{\partial \phi_j}{\partial y_j} = \tau^y_{i,j} + \xi_i \tau^\phi_{i,j}\frac{1}{\rho} \tag{4}$$

This equation describes the change of y at any location i due to the change of y at a given master point j. It should be noted that the second term is set to zero if $\rho = 0$; then collocated kriging equation becomes simple kriging equation.

Based on this, we can build in the correlation relationship into flow equation to get sensitivity of pressure on y and ϕ. Details are as follows:

Discretization of flow equation with an implicit scheme leads to the following equation:

$$\mathbf{A}\mathbf{p}^{n+1} = \mathbf{B}\mathbf{p}^n + \mathbf{f}^n \tag{5}$$

$\mathbf{A}$, $\mathbf{B}$, and $\mathbf{f}$ have close form equation. It is possible to obtain derivatives of $\mathbf{A}$, $\mathbf{B}$, and $\mathbf{f}$ with respect to y. A point to be noted that $\mathbf{A}$ and $\mathbf{B}$ are explicit functions of $k = \exp(y)$, and only the diagonal terms of these matrices have terms depending on ϕ. However, since y is correlated to ϕ (as shown in Equation 2), non-diagonal terms of both $\mathbf{A}$ and $\mathbf{B}$ are also dependent on ϕ implicitly. Thus, we need to extend this to include ϕ being a variable as well.

Elements of $\mathbf{A}$ are the sum of transmissibilities. Using geometry averages of permeabilities in the transmissibility calculation in the code, we have for any two adjacent grid cells 1 and 2

$$T_{1,2} = \sqrt{k_1 k_2} = \exp\left\{\frac{y_1 + y_2}{2}\right\} \tag{6}$$

where $y_1 = \log(k_1)$ and $y_2 = \log(k_2)$. Consequently, the derivatives are computed as

$$\frac{\partial T_{1,2}}{\partial y_j} = \frac{1}{2} T_{1,2}\left(\frac{\partial y_1}{\partial y_j} + \frac{\partial y_2}{\partial y_j}\right) \tag{7}$$

The sensitivity coefficients in the above equation can be calculated using (4).

For terms of $\mathbf{A}$ and $\mathbf{B}$ having ϕ variable, we need

$$\frac{\partial \phi_i}{\partial y_j} = \frac{\partial \phi_i}{\partial \phi_j}\frac{\partial \phi_j}{\partial y_j} = \frac{\tau^\phi_{i,j}}{\rho} \tag{8}$$

Again right hand side of the above equation is set to 0 when $\rho = 0$. Using Equations 7 and 8, we can compute derivatives of $\mathbf{A}$, $\mathbf{B}$, and $\mathbf{f}$ with respect to y, and obtain the sensitivity of pressure on y, i.e., $\partial p_i / \partial y_j$.

The sensitivity of pressure on porosity can be similarly calculated. In order to compute derivatives of $\mathbf{A}$, $\mathbf{B}$, and $\mathbf{f}$ with respect to ϕ at any master point j, we need the sensitivity coefficients of y_i with respect to ϕ_j. Applying Equation 4 and chain rule, we have

$$\frac{\partial y_i}{\partial \phi_j} = \frac{\partial y_i}{\partial y_j}\frac{\partial y_j}{\partial \phi_j} = \rho \frac{\partial y_i}{\partial y_j} = \rho\left(\tau^y_{i,j} + \xi_i \tau^\phi_{i,j}\frac{1}{\rho}\right) = \rho \tau^y_{i,j} + \xi_i \tau^\phi_{i,j} \tag{9}$$

Introducing above relationships into the derivative of Equation 5, engenders:

$$\frac{\partial p_i}{\partial \phi_j} = \frac{\partial p_i}{\partial y_j}\frac{\partial y_j}{\partial \phi_j} = \rho \frac{\partial p_i}{\partial y_j} \tag{10}$$

It is observed from the above relationship that we do not need to solve equation again to get sensitivity coefficient of porosity, but just using the linear regression relationship to get the sensitivity coefficients of the response variables with respect to ϕ from those with respect to y. Again when $\rho = 0$, Equation 10 can not be used, and we need to use 9 to compute the derivatives in Equation 5 to get the sensitivity coefficients with respect to porosity. Such calculation would be simple since there is no permeability term. It is now possible to perform the optimization to find the optimal Δy_j and $\Delta \phi_j$, $j = 1, \ldots, n_{mp}$.

Having performed the optimization, we propagate the optimal perturbations into the entire domain using collocated cokriging (Equations 1 and 2).

Thus, the algorithm for the simultaneous porosity and permeability inversion is laid out below.

1. Selection of master points.
2. Performing simple (or ordinary) kriging on ϕ to get kriging weights $\tau^{\phi}_{i,j}$ at a location i for $\phi_j,\ j = 1, \ldots, n_{mp}$.
3. Collocated cokriging with Markov-type assumption and obtain cokriging weights $\tau^{y}_{i,j}$ and ξ_i.
4. Solution of pressure equations.
5. Computing derivatives of matrices in Equation 5 with respect to y_j for all master points.
6. Computing sensitivity coefficients with respect to y.
7. Computing sensitivity coefficients with respect to ϕ using Equation 10 or 9.
8. Performing optimization to compute optimal change of Δy_j and $\Delta \phi_j$.
9. Propagating changes into entire domain.
10. Updating initial ϕ and y fields.
11. Repeating Step (1) to (10) till convergence is achieved.

Thus, a methodology has been developed for simultaneous inversion of porosity and permeability. The algorithm for computing the sensitivity coefficients is based on kriging equation for porosity and collocated cokriging equation for permeability modeling in the framework of Sequential Self-Calibration technique. It essentially utilizes the geostatistical correlation involved in the kriging equations and permeability sensitivity of the pressure equation. This approximation reduces drastically the computation time for the porosity sensitivity and permeability sensitivity of the flow responses separately.

Application of the Algorithm

A synthetic example is used here to evaluate the ability of the algorithm to generate models of porosity and permeability from multiple well production data. In this example, first, reference porosity and permeability models are constructed, and then, the dynamic pressure responses at a number of wells, caused by changing flow rates, are obtained by flow simulation. On the basis of dynamic flow rate and pressure data and information on the variograms of porosity and permeability, the new algorithm is used to invert for both porosity and permeability fields that match the production data. Then, the inverted fields are compared with the reference field to evaluate the capability of the algorithm.

Example 1. This example is a 2D, 4,000-ft^2 domain that is discretized into 25 $\times$ 25 grid cells of 160 $\times$ 160 ft. There is a high porosity (0.25) and high permeability (500 mD) band connecting the lower-left corner and upper-right corner. The porosity and the permeability in other areas are 0.175 and 10 mD, respectively. Figure 1 shows the reference porosity and permeability fields. There are four wells: W1 at the center of the cell (5,21), W2 at (21,21),W3 at (5,5), and W4 at (21,5). The four boundaries are no-flow boundaries, reservoir thickness is 100 ft, viscosity is 0.2 cp, formation compressibility is 10^{-6} psi^{-1}, and well radius is 0.3 ft. For global distribution (histogram) of porosity and permeability, we have used bimodal distributions that are present in the reference field.

Figure 2 shows the imposed producing rates and the corresponding pressure responses at the different wells solved numerically. Different shut-in times for different wells are intended to create some well interference so that more information on spatial variations of permeability is contained in the production data.

Simultaneous porosity and permeability inversion can be difficult if not impossible in many cases. Conflicting information of various data contributes to a suite of options for the implementation. The present code facilitates the option of using production data and other hard petrophysical information in terms local hard data or global distribution, mainly histogram. Results obtained using various

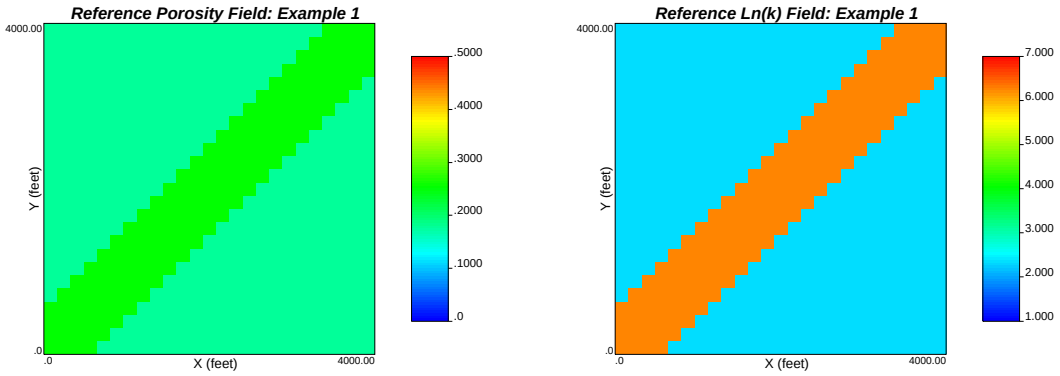

Figure 1: Reference deterministic porosity and permeability fields: Example 1.

options are informative. On the basis of production and pressure data at the four wells, the new method was used to estimate the spatial distribution of both porosity and permeability. Inverted models from runs with various options are discussed and analyzed below. Sensitivity of the inverted models to the selection of various anisotropy, initial fields, optimization parameters, search radii, and so forth will be demonstrated later.

For all the runs below, we used initial porosity and permeability fields of $\phi = 0.4$ and $\ln(k) = 3.15$ ln(mD), respectively. From prior information on variography, anisotropic variograms with very long correlation length (about 8,000 ft) in the 45^0 direction for both porosity and permeability were employed. All data and parameter files required for the runs are provided in the appendix.

- **Run 1: Inversion with production data, global histogram, prior information on variography, and local hard data.**

  Local hard data considered are porosity values of 0.175, 0.25, 0.25, and 0.175 for cells (5,21), (21,21),(5,5), and (21,5) respectively. Permeability values for the same cells are 2.3026, 6.2146, 6.2146, and 2.3026 ln(mD) respectively.

  The inverted models are obtained after 17 outer iterations (75 seconds in 733 MHz dual processor workstation). The pressure responses in the updated porosity and permeability fields converge to the reference pressure data. These inverted models are shown in Figure 3. The spatially connected high porosity/permeability bands connecting W2 and W3 are clearly evident. Figure 4 shows the pressure values at the four wells computed from the true (from reference), initial and final updated porosity and permeability fields. Pressure responses in the initial field deviate significantly from the true values because of the poor model; however, the updated fields by the new method accurately reproduces the true pressure data at all wells. The objective function values of the inversion process is shown in Figure 5. Final average pressure mismatch (in L^2 norm sense) for 200 data was 4.1 psi, which is remarkably small as evident from the pressure match in Figure 4. Updated porosity and permeability fields after each outer iteration of the inversion method are shown in Figures 6 and 7. Number of function evaluation in the inner optimization loop for each outer iteration are shown in Figure 8. It should be noted that number of function evaluation curve gives information on the termination criteria having been met or not. If the number of function evaluation is at the assigned minimum then it can said that either objective function termination criterion or gradient termination criterion has been met. On the other hand, curve of the norm of the objective function gradient gives an indication of the amount of change taken place in the inner optimization module at the termination of each outer iteration. Higher norm values imply more changes in the solution space. Norm of objective function gradient in the inner optimization loop at each outer iteration is shown in Figure 9. More information could be derived from the gradient curves of the

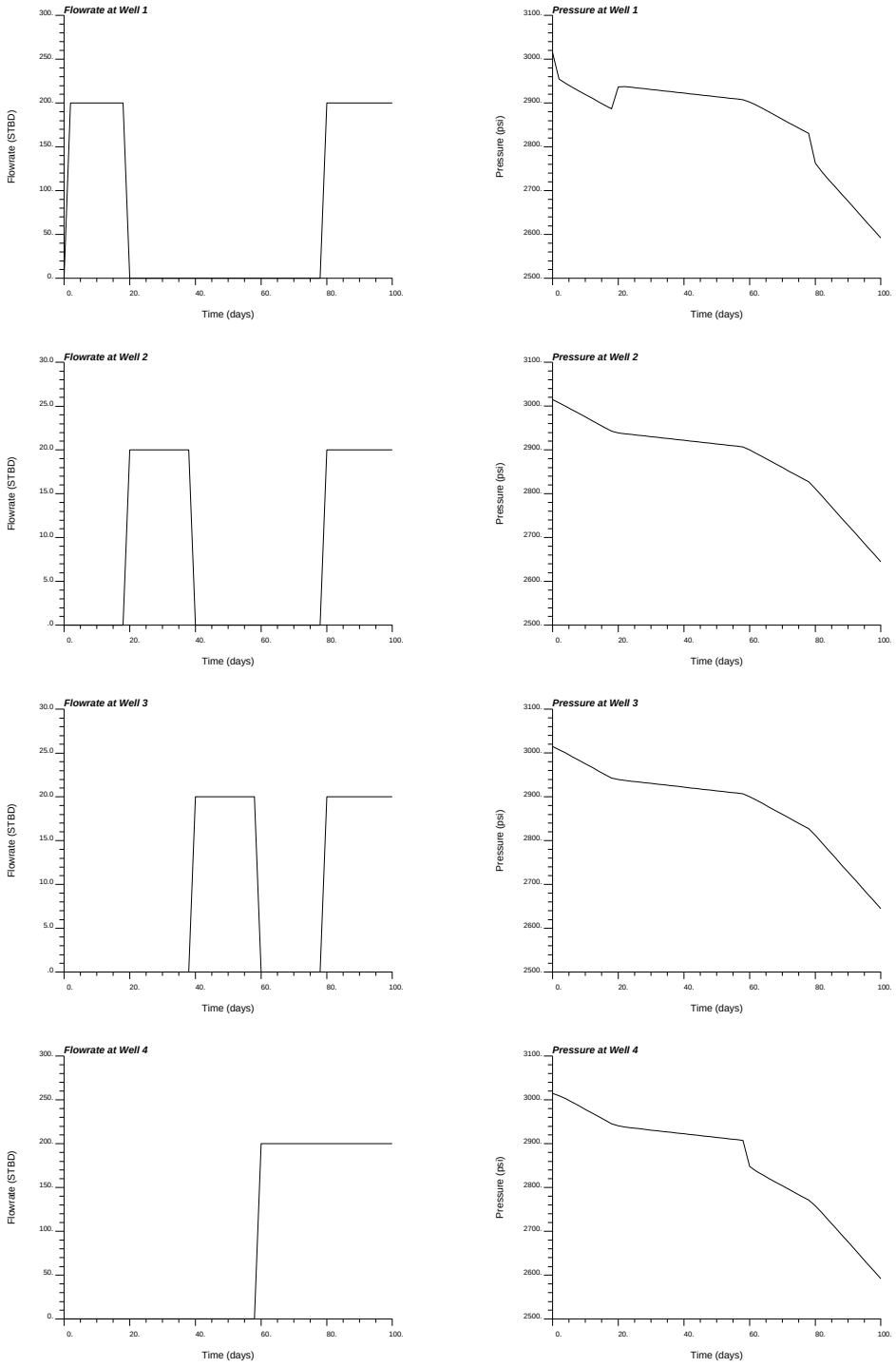

Figure 2: Production data (both pressure and flow rates) obtained from the reference field: Example 1.

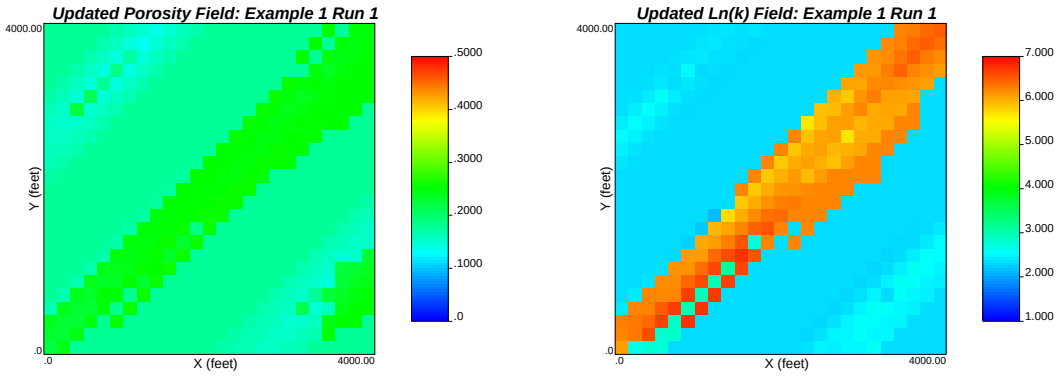

Figure 3: Updated porosity and permeability fields honoring production data, local gard data, global distribution and prior variography information : Example 1 Run 1.

objective function with respect to Master Point porosity and permeabilities. These gradient curves of the objective function at each outer iteration are shown in Figure 10. Analyzing these curves, one can identify the which Master Points are more effective in the inner optimization subproblem. One could also determine variations in the sensitivities at each outer iteration.

At this point, it would be interesting to see how the porosity and permeability models and their pressure responses when only only static information is used. Figure 11 shows the conditionally simulated porosity and permeability fields using local hard data, prior global distribution and information on variography. So, no production data information is captured in these models. The models themselves appear to have the major features of the reference models. However, the pressure responses (shown in Figure 12) computed from these models deviate from those in the reference field significantly.

If the global distribution is not used in static inversion (conditional simulation), the models and their pressure responses deviate drastically from the reference model. Figure 13 shows these conditionally simulated porosity and permeability fields. Figure 14 shows the computed pressure responses of these models. Comparison with these conditionally simulated models with the models inverted using production data gives us an idea of what information can be resolved and how much of it by using production data. It is important to realize that more data we integrate, the better resolved the model. On the contrary, it must also be understood that information from different data can be conflicting and the algorithm we develop cannot implement global optimality criteria. Thus, sometimes in spite of using more data we are stuck with a poor model due to lack of convergence to the global minima and conflicting information.

- **Run 2: Inversion with production data, global histogram, prior information on variography, but no local hard data.**

  The inverted models are obtained after 5 outer iterations (26 seconds in 733 MHz dual processor workstation). The pressure responses in the updated porosity and permeability fields converge to the reference pressure data. These inverted models are shown in Figure 15. The spatially connected high porosity/permeability bands connecting W2 and W3 are clearly evident. Figure 16 shows the pressure values at the four wells computed from the true (from reference), initial and final updated porosity and permeability fields. Interesting to note that pressure match in this case is even better than the previous case. Pressure responses in the updated fields by the new method accurately reproduces the true pressure data at all wells. The objective function values of the inversion process is shown in Figure 17. Final average pressure mismatch (in L^2 norm sense) for 200 data was 1.7 psi (compared to 4.1 psi in Run 1). However, close inspection of the final models tells us that these models do not accurately capture the major features in the reference field. Updated porosity and permeability fields after each outer iteration of the

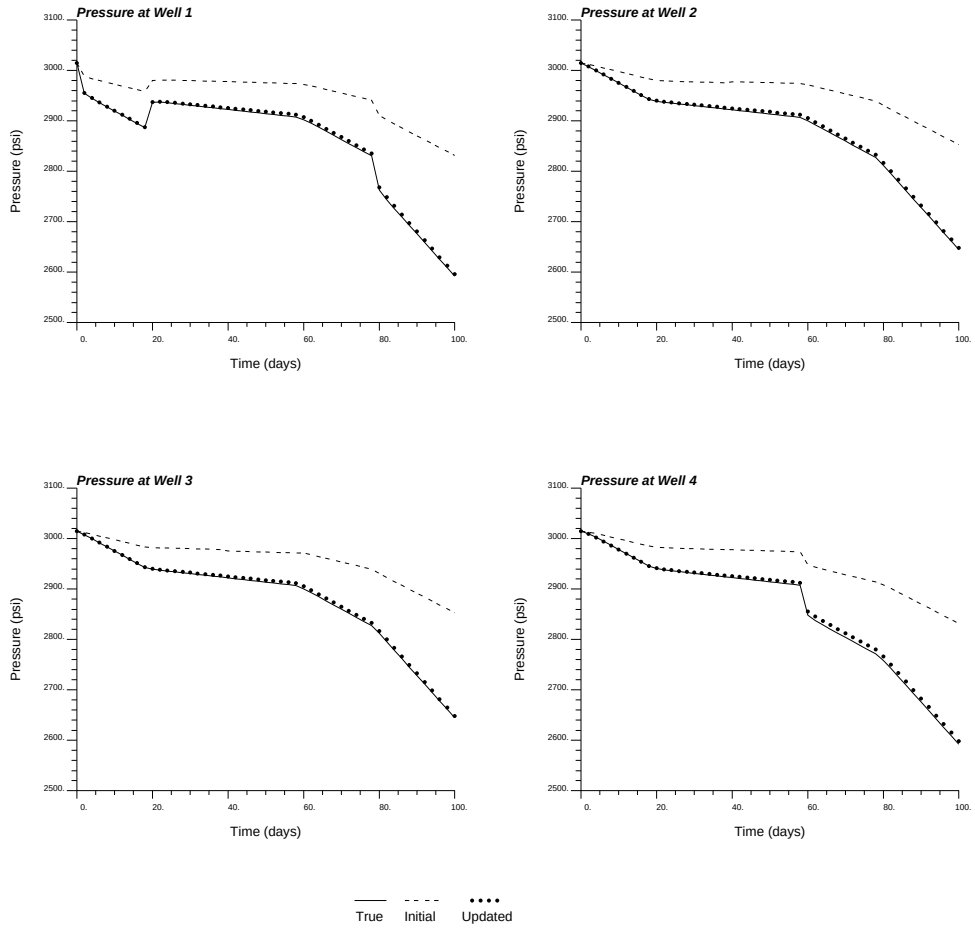

Figure 4: The pressure responses computed from intial (dashed lines) and updated (bullets) porosity and permeability fields with the true data (solid lines) : Example 1 Run 1.

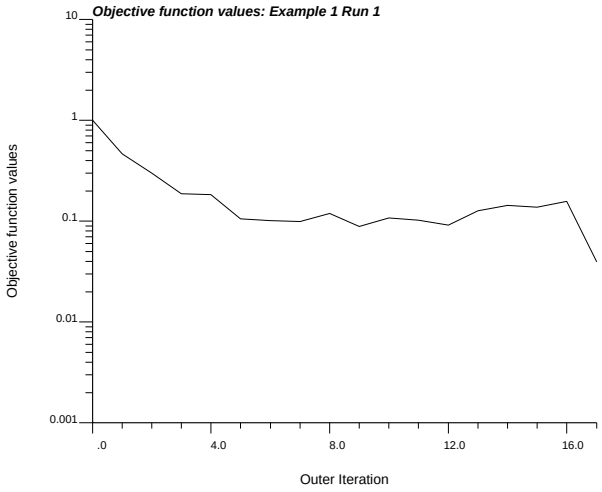

Figure 5: Objective function values of the simultaneous inversion process : Example 1 Run 1.

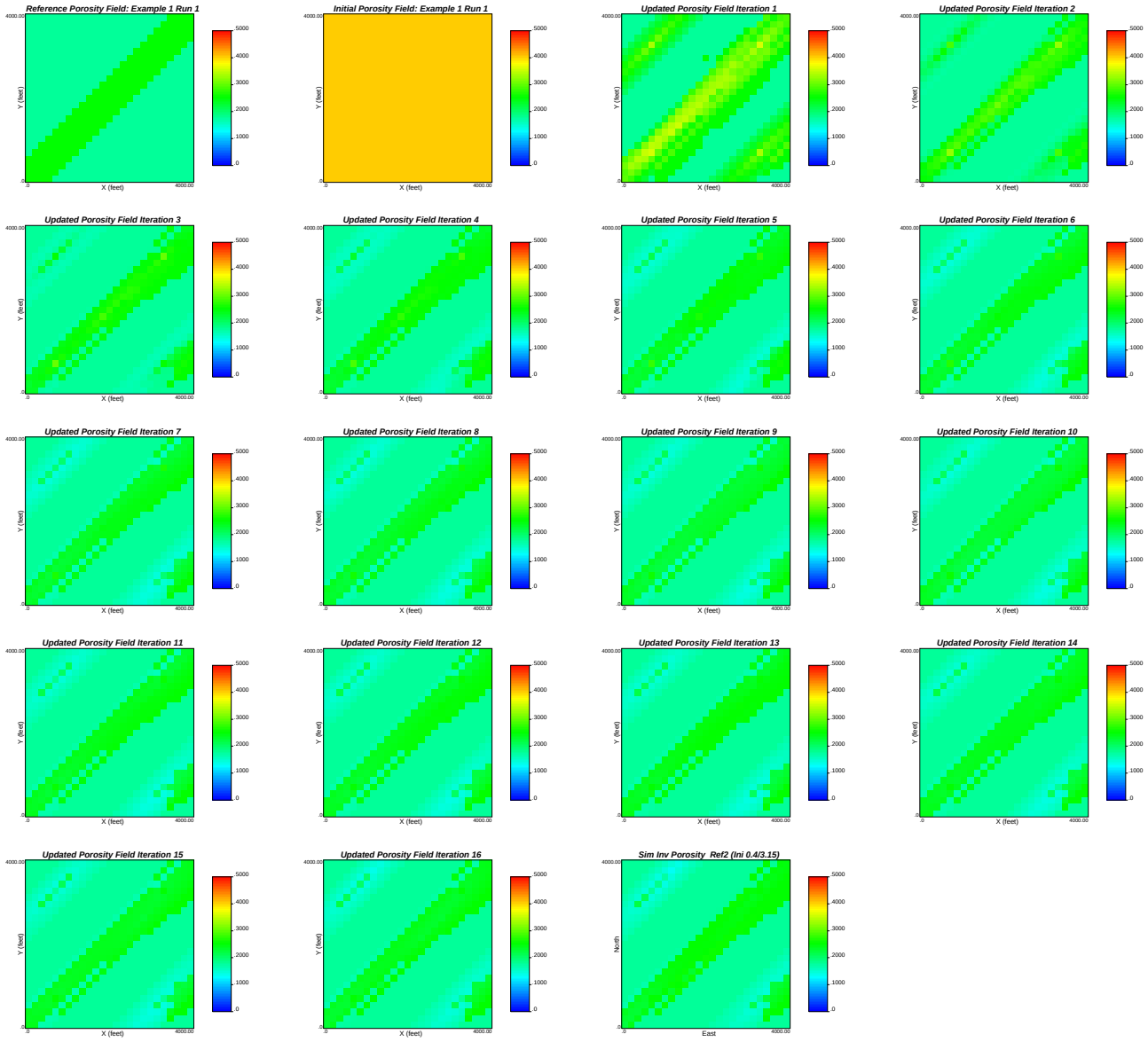

Figure 6: Updated porosity fields at each iteration of the simultaneous inversion process : Example 1 Run 1.

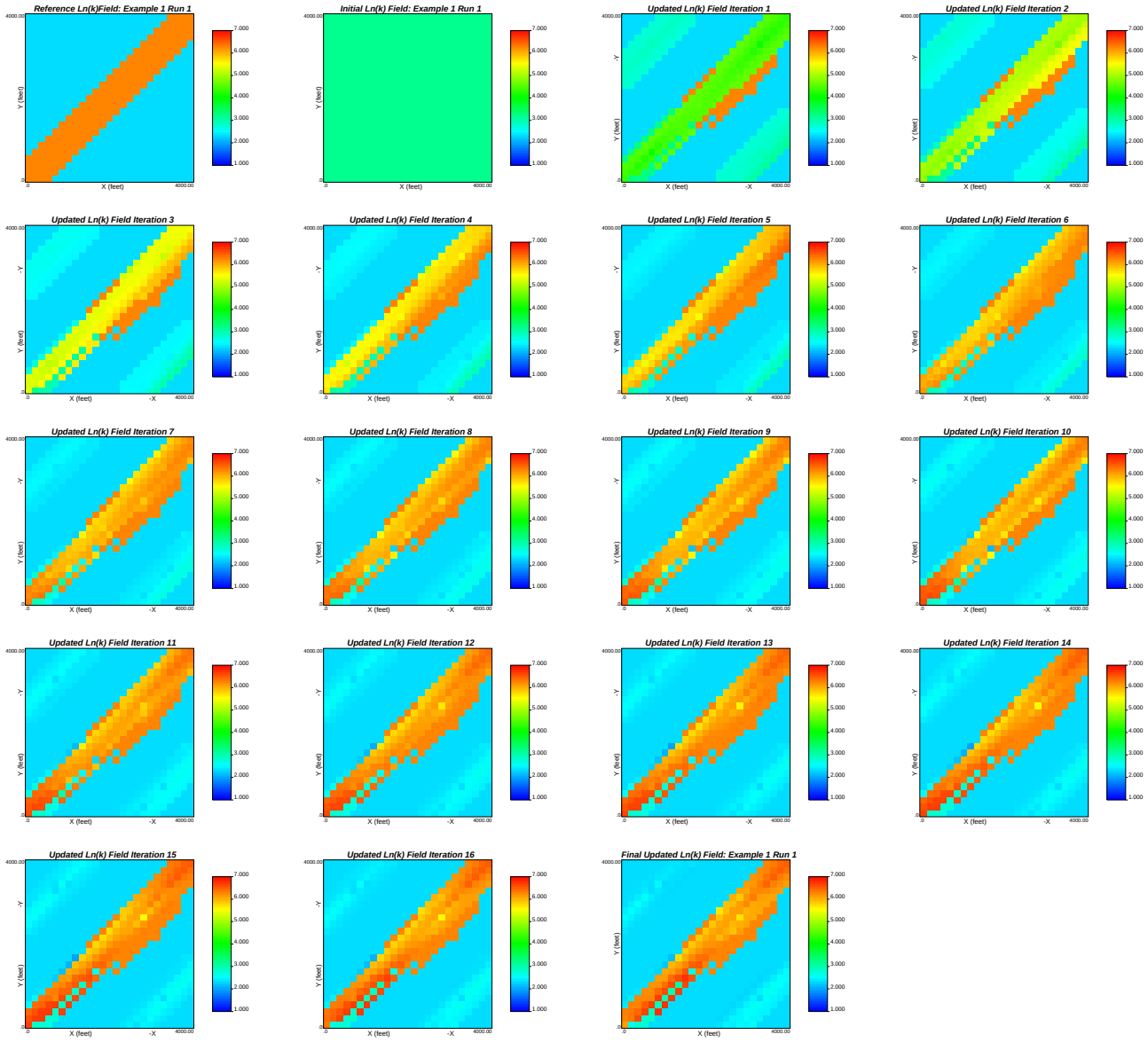

Figure 7: Updated Ln(k) fields at each iteration of the simultaneous inversion process : Example 1 Run 1.

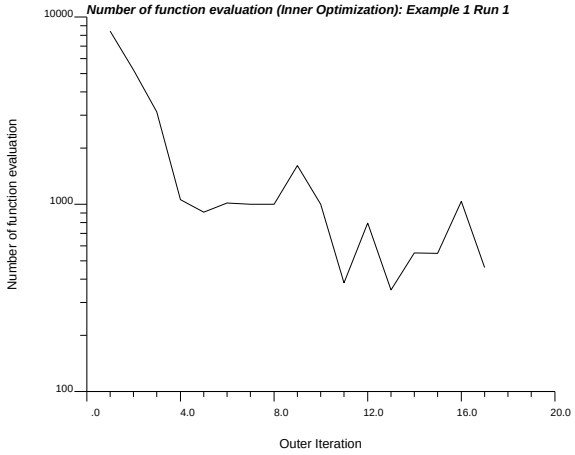

Figure 8: Number of function evaluation in the inner optimization loop for each outer iteration: Example 1 Run 1.

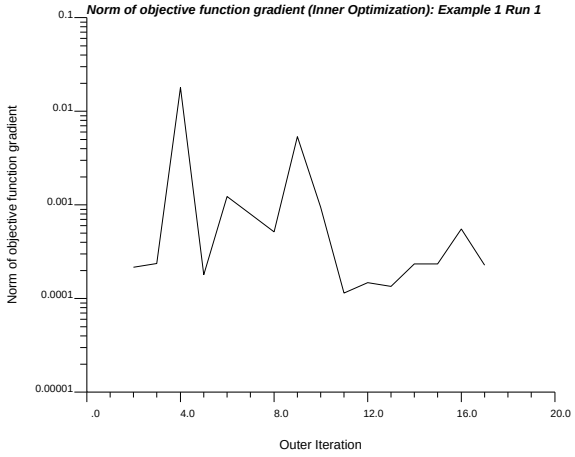

Figure 9: Norm of objective function gradient in the inner optimization loop at each outer iteration: Example 1 Run 1.

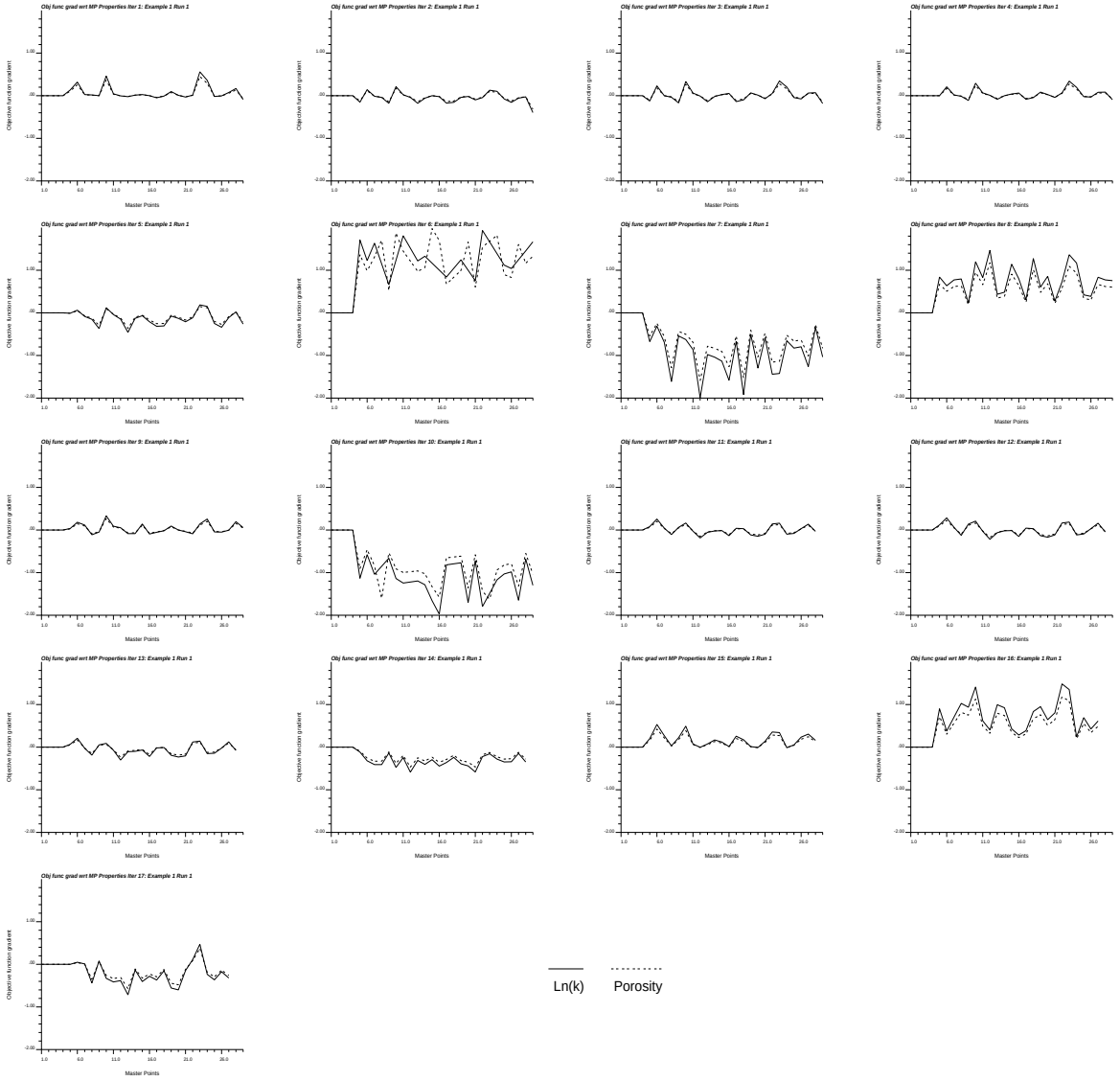

Figure 10: Gradient of the objective function with respect to Master Point permeability (solid lines) and porosity (dashed lines) at each outer iteration: Example 1 Run 1.

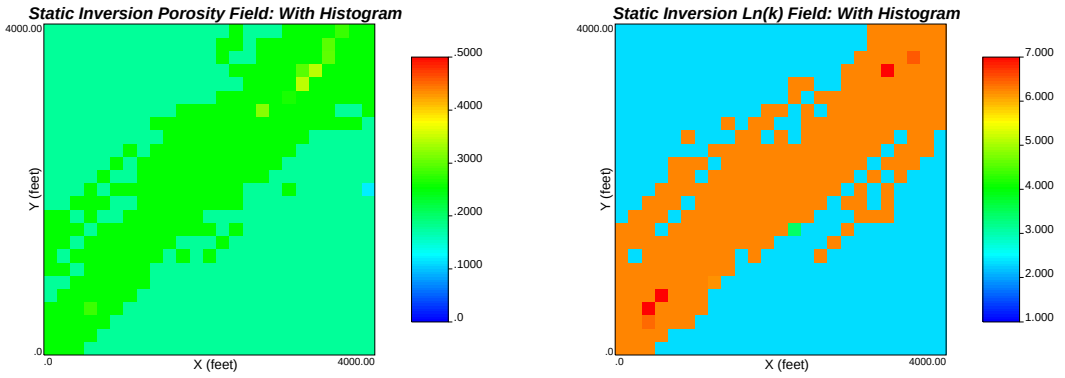

Figure 11: Conditional simulation of porosity and permeability fields honoring local gard data, global distribution and prior variography information, but no production data is used.

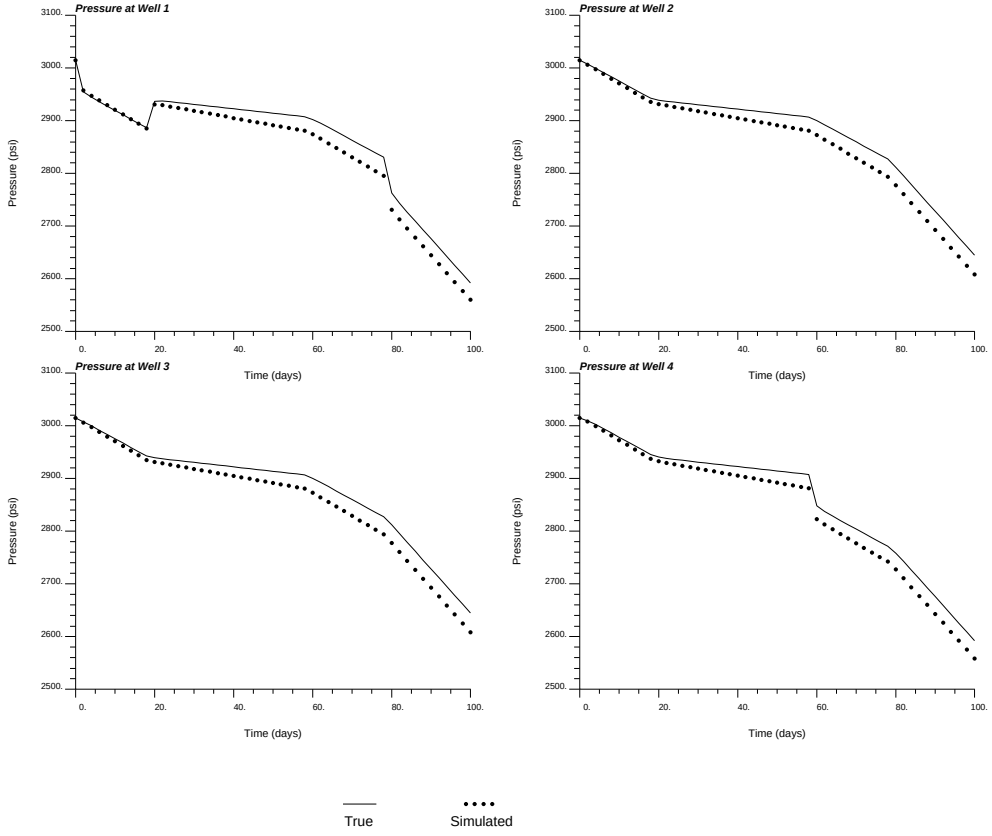

Figure 12: The pressure responses computed from conditionally simulated (bullets) porosity and permeability fields with the true data (solid lines).

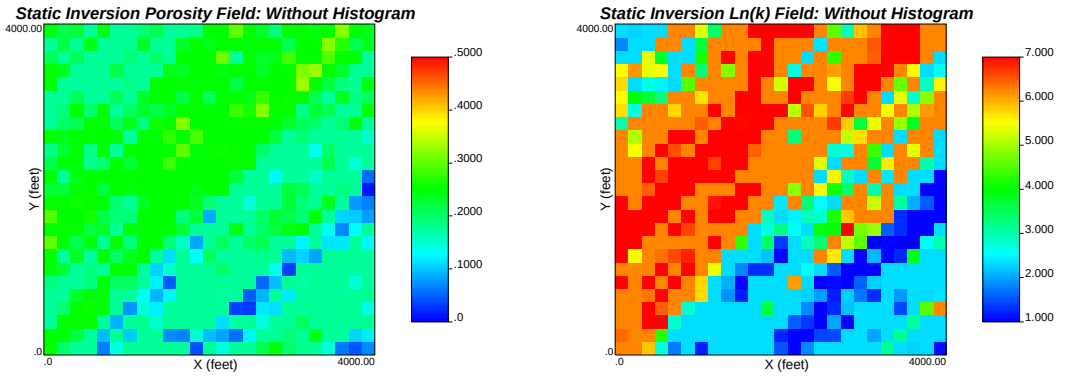

Figure 13: Conditional simulation of porosity and permeability fields honoring local gard data, and prior variography information, but no global distribution or production data is used.

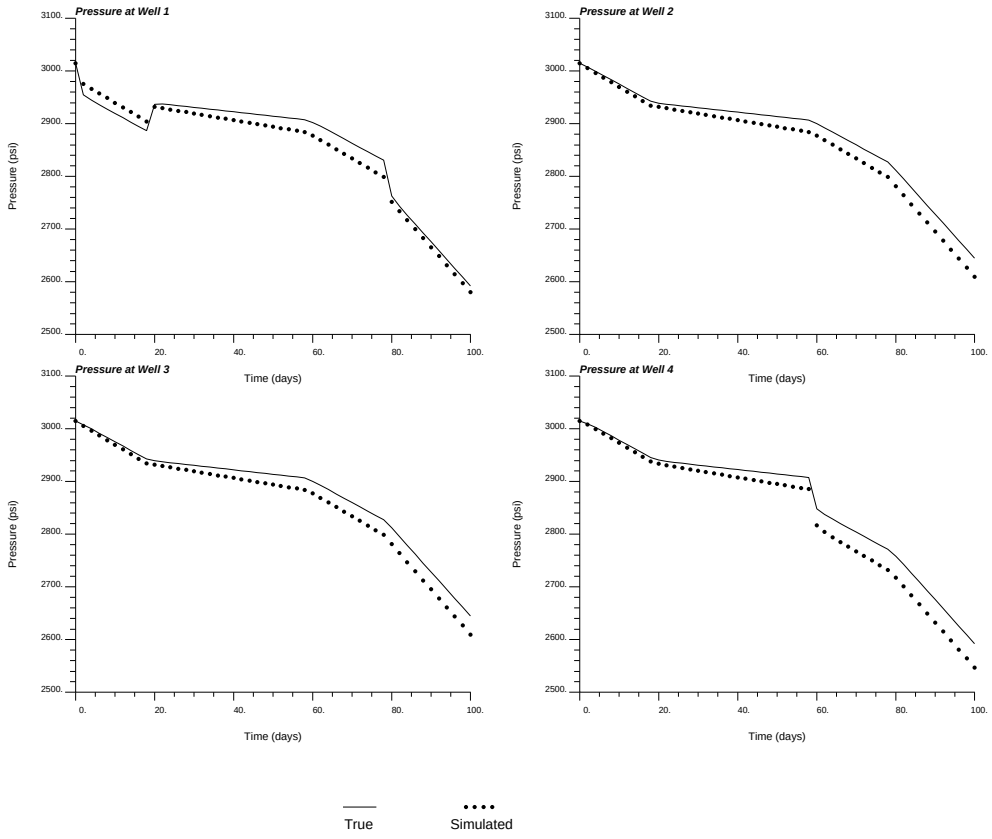

Figure 14: The pressure responses computed from conditionally simulated (bullets) porosity and permeability fields with the true data (solid lines).

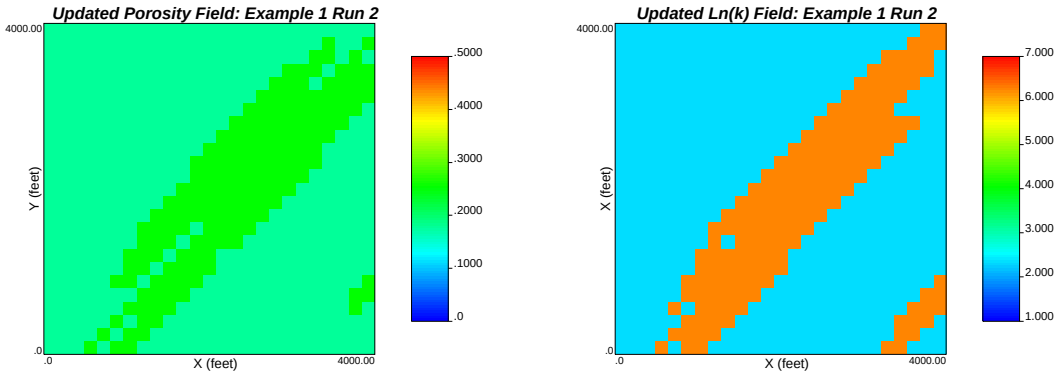

Figure 15: Updated porosity and permeability fields honoring production data, global distribution and prior variography information but no local hard data : Example 1 Run 2.

inversion method are shown in Figures 18 and 19. In fact, the inner optimization gets confined in a local minima within first the outer iteration. This is evident from the curves of number of function evaluation and norm of objective function gradient in the inner optimization loop. Number of function evaluation in the inner optimization loop for each outer iteration are shown in Figure 20. Norm of objective function gradient in the inner optimization loop at each outer iteration is shown in Figure 21. The gradient of the objective function at each outer iteration is shown in Figure 22.

- **Run 3: Inversion with production data, prior information on variography and local hard data, but no global distribution.**

  Local hard data are employed same as those considered in the Run 1. These are porosity values of 0.175, 0.25, 0.25, and 0.175 for cells (5,21), (21,21),(5,5), and (21,5) respectively. Permeability values for the same cells are 2.3026, 6.2146, 6.2146, and 2.3026 ln(mD) respectively.

  The inverted models are obtained after 7 outer iterations (44 seconds in 733 MHz dual processor workstation). The pressure responses in the updated porosity and permeability fields converge to the reference pressure data. These inverted models are shown in Figure 23. The spatially connected high porosity/permeability bands connecting W2 and W3 are clearly evident. Figure 24 shows the pressure values at the four wells computed from the true (from reference), initial and final updated porosity and permeability fields. The objective function values of the inversion process is shown in Figure 25. Final average pressure mismatch (in L^2 norm sense) for 200 data was 9.1 psi. Compared to the first two runs, this is a relatively high number. Updated porosity and permeability fields after each outer iteration of the inversion method are shown in Figures 26 and 27. Number of function evaluation in the inner optimization loop for each outer iteration are shown in Figure 28. Norm of objective function gradient in the inner optimization loop at each outer iteration is shown in Figure 29. The gradient of the objective function at each outer iteration is shown in Figure 30. Having observed these graphs and the pressure mismatch curves, it can be said that prior information of global distribution is important in the inversion process.

- **Run 4: Inversion with production data and prior information on variography, but no local hard data or global distribution.**

  The inverted models are obtained after 10 outer iterations (47 seconds in 733 MHz dual processor workstation). The pressure responses in the updated porosity and permeability fields converge to the reference pressure data. These inverted models are shown in Figure 31. The spatially connected high porosity/permeability bands connecting W2 and W3 are clearly evident. Figure 32 shows the pressure values at the four wells computed from the true (from

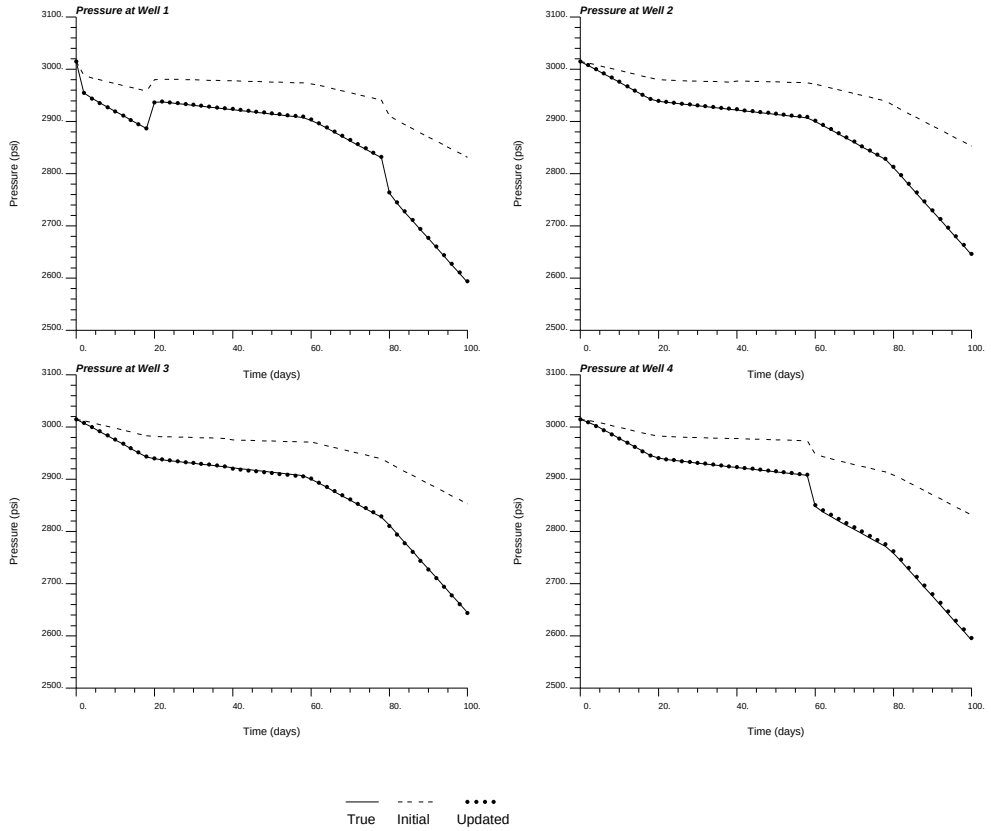

Figure 16: The pressure responses computed from intial (dashed lines) and updated (bullets) porosity and permeability fields with the true data (solid lines) : Example 1 Run 2.

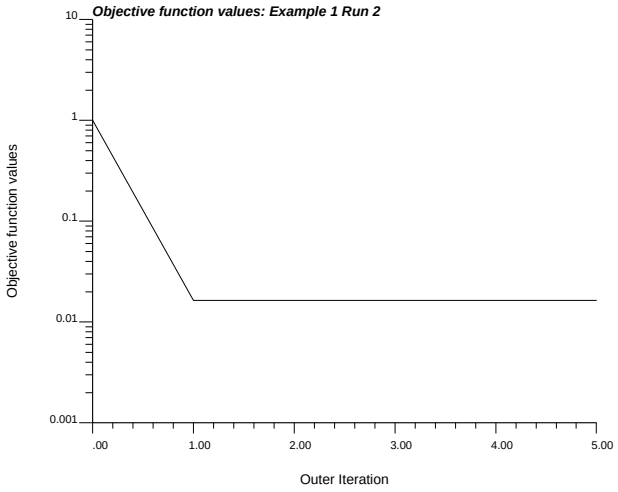

Figure 17: Objective function values of the simultaneous inversion process : Example 1 Run 2.

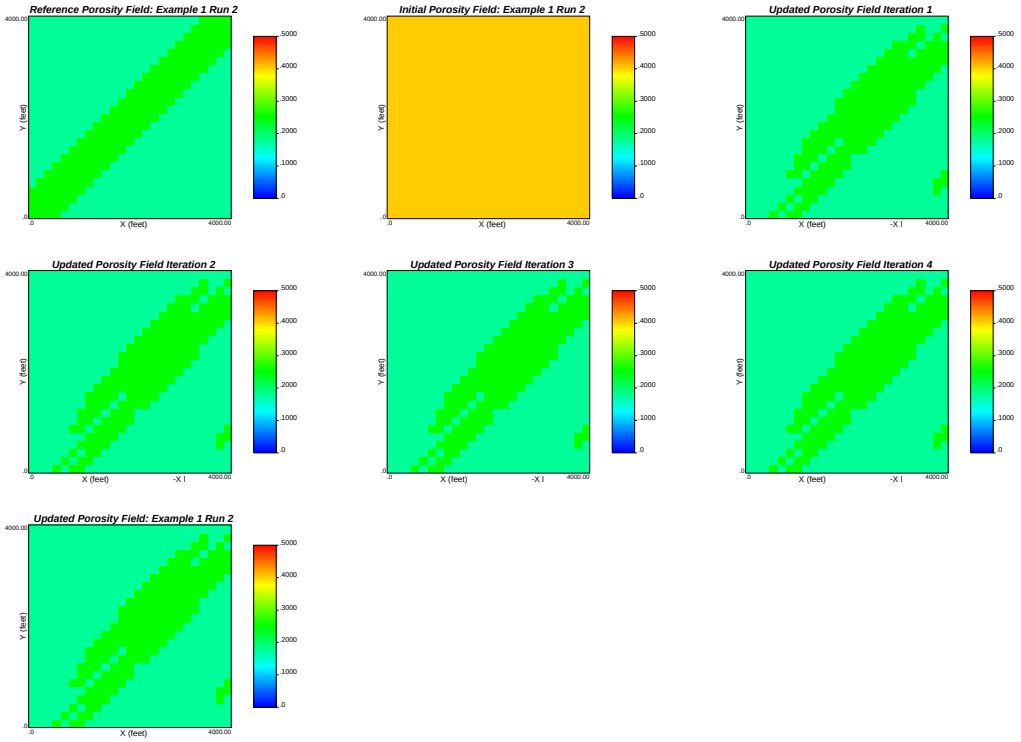

Figure 18: Updated porosity fields at each iteration of the simultaneous inversion process : Example 1 Run 2.

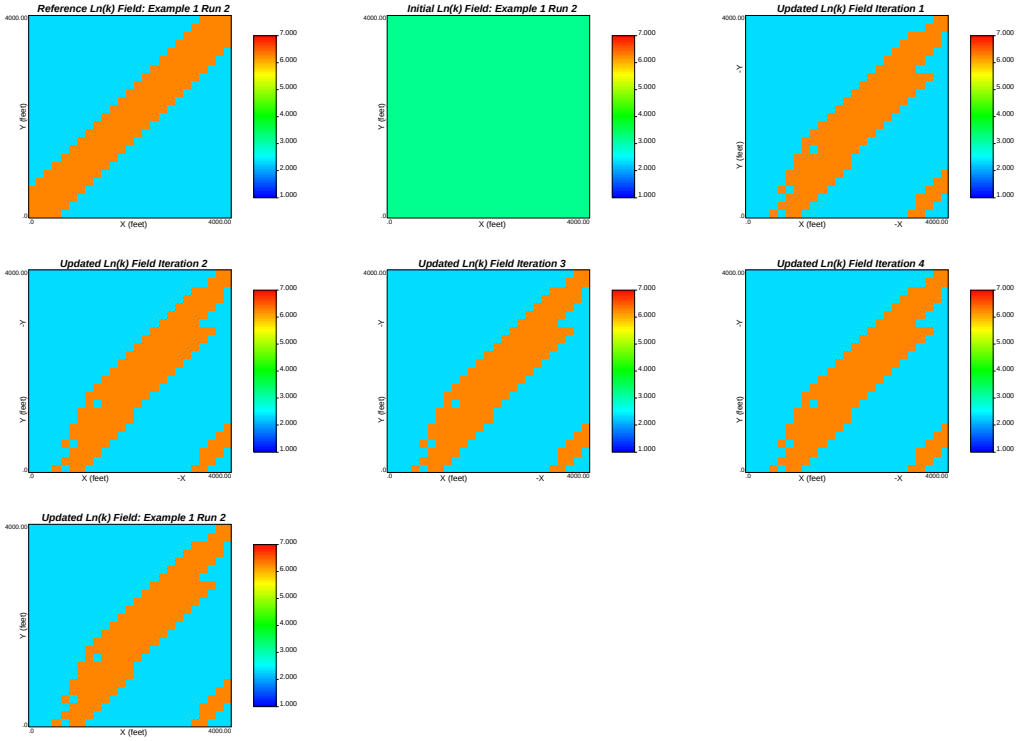

Figure 19: Updated Ln(k) fields at each iteration of the simultaneous inversion process : Example 1 Run 2.

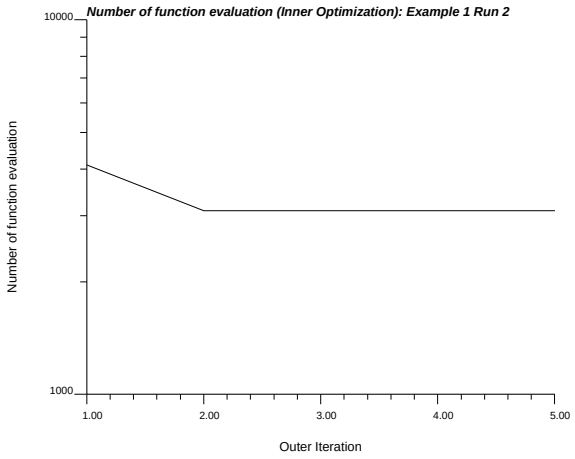

Figure 20: Number of function evaluation in the inner optimization loop for each outer iteration: Example 1 Run 2.

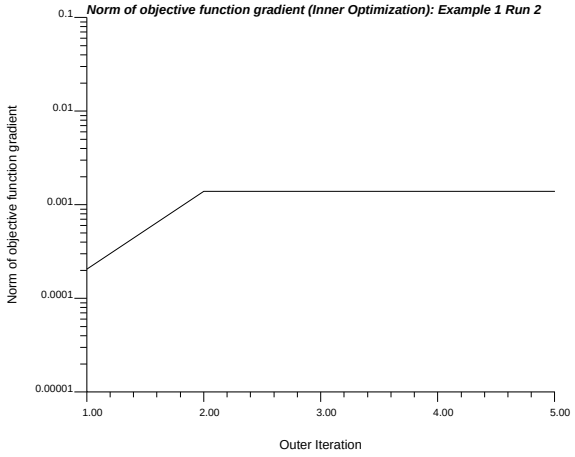

Figure 21: Norm of objective function gradient in the inner optimization loop at each outer iteration: Example 1 Run 2.

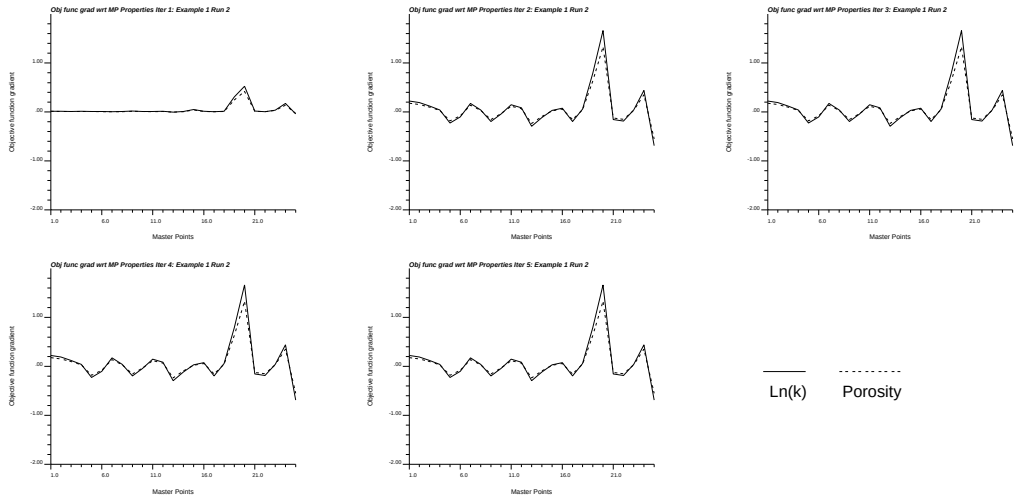

Figure 22: Gradient of the objective function with respect to Master Point permeability (solid lines) and porosity (dashed lines) at each outer iteration: Example 1 Run 2.

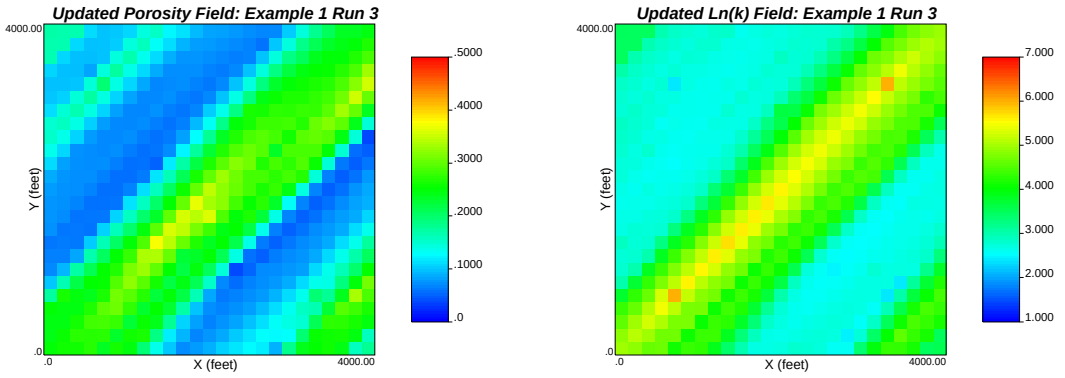

Figure 23: Updated porosity and permeability fields honoring production data, local hard data and prior variography information but no global distribution : Example 1 Run 3.

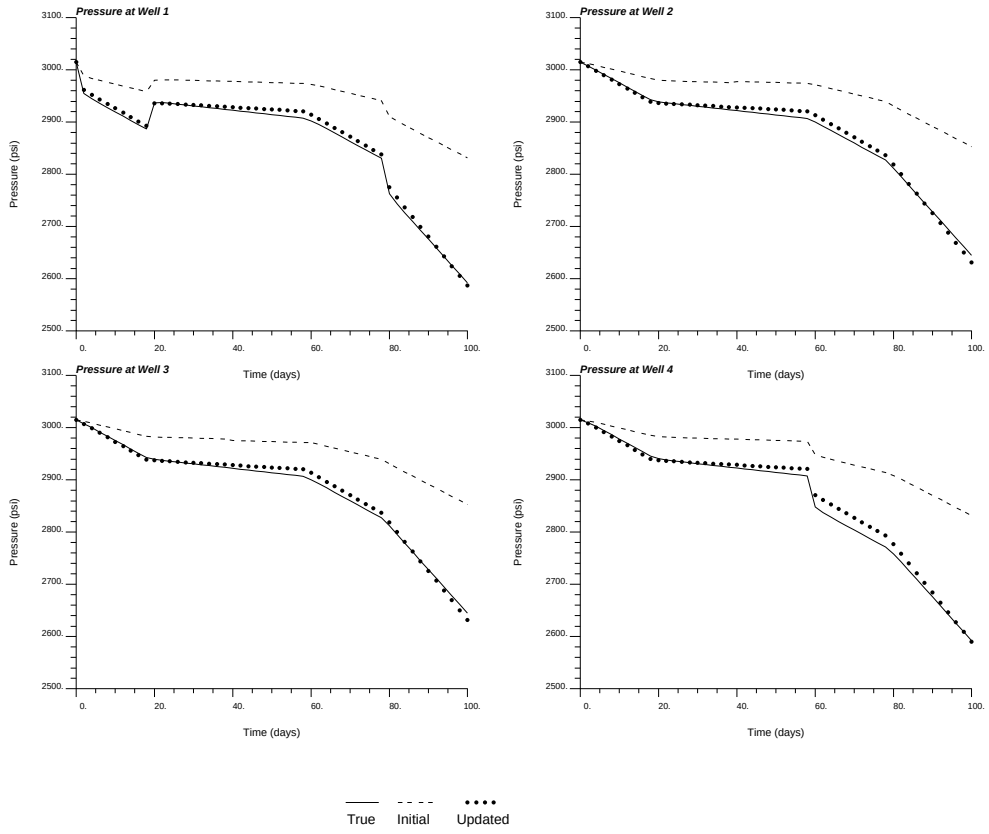

Figure 24: The pressure responses computed from intial (dashed lines) and updated (bullets) porosity and permeability fields with the true data (solid lines) : Example 1 Run 3.

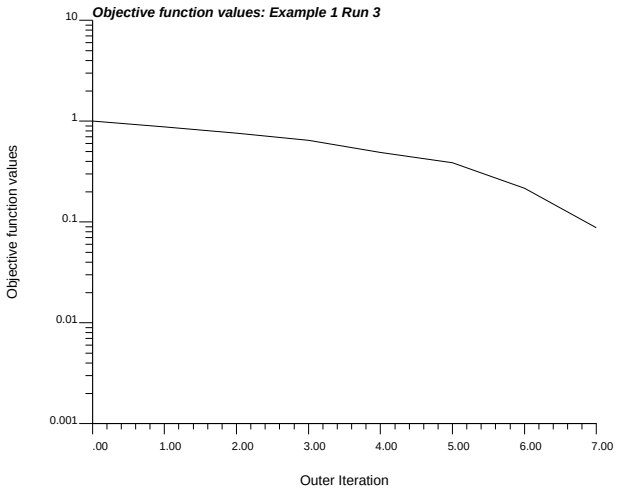

Figure 25: Objective function values of the simultaneous inversion process : Example 1 Run 3.

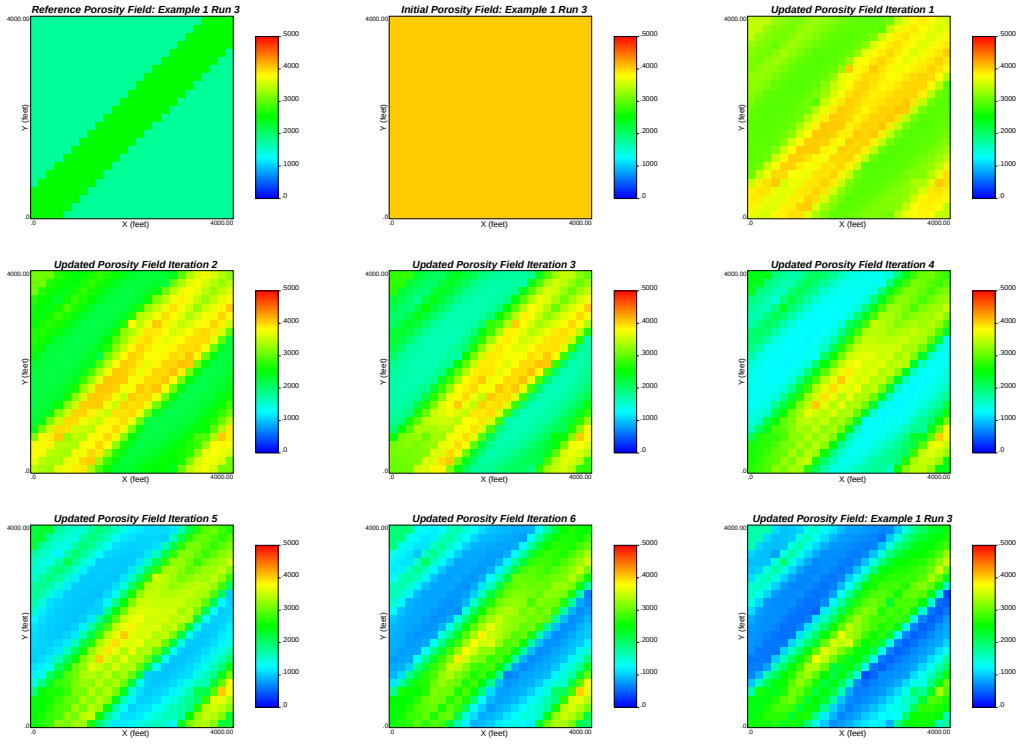

Figure 26: Updated porosity fields at each iteration of the simultaneous inversion process : Example 1 Run 3.

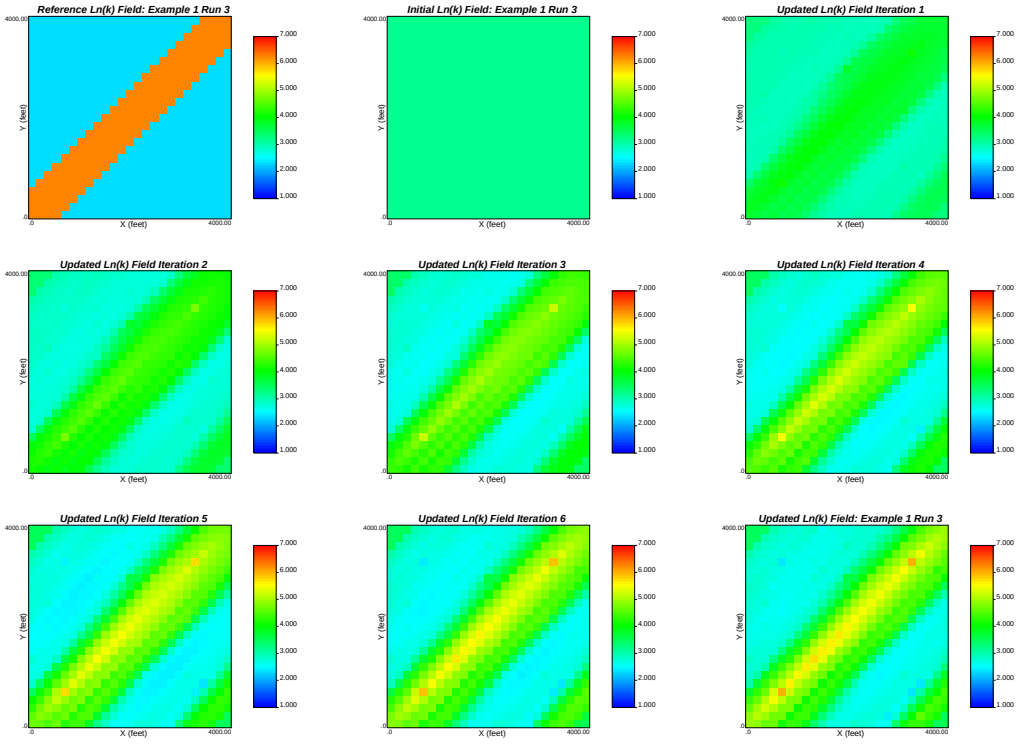

Figure 27: Updated Ln(k) fields at each iteration of the simultaneous inversion process : Example 1 Run 3.

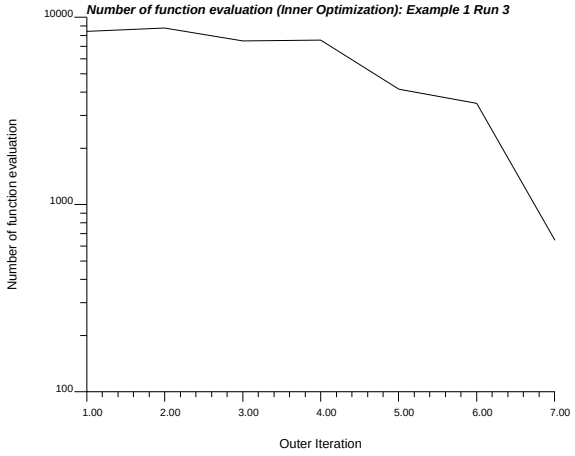

Figure 28: Number of function evaluation in the inner optimization loop for each outer iteration: Example 1 Run 3.

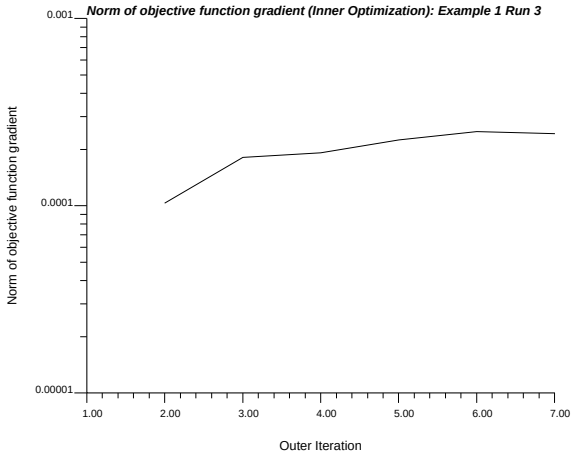

Figure 29: Norm of objective function gradient in the inner optimization loop at each outer iteration: Example 1 Run 3.

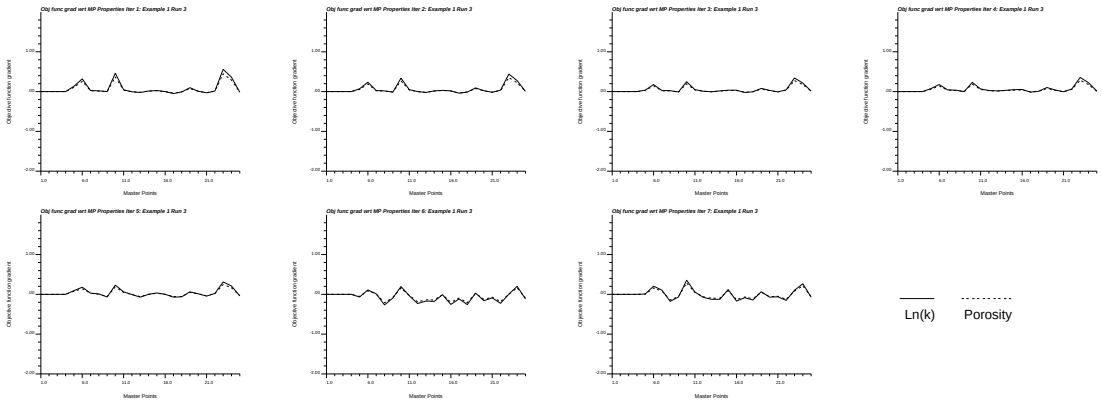

Figure 30: Gradient of the objective function with respect to Master Point permeability (solid lines) and porosity (dashed lines) at each outer iteration: Example 1 Run 3.

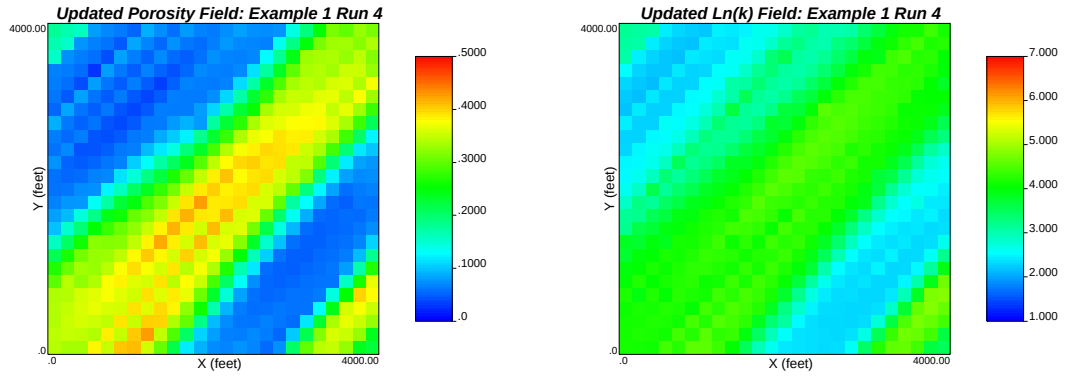

Figure 31: Updated porosity and permeability fields honoring production data, and prior variography information but no local hard data or global distribution : Example 1 Run 4.

reference), initial and final updated porosity and permeability fields. The objective function values of the inversion process is shown in Figure 33. Final average pressure mismatch (in L^2 norm sense) for 200 data was 33.3 psi, which is a relatively high value. This poor match is evident in the pressure match in Figure 32. Updated porosity and permeability fields after each outer iteration of the inversion method are shown in Figures 34 and 35. Number of function evaluation in the inner optimization loop for each outer iteration are shown in Figure 36. Norm of objective function gradient in the inner optimization loop at each outer iteration is shown in Figure 37. Examining the norm of the objective function gradient, it can inferred that outer optimization has not reached the region of a minima. In fact, the gradients of the objective function at each outer iteration (shown in Figure 38) are significantly low to arrive at the minima. This is natural to expect this poor match and model generation with only information from production data but no hard information of local or global spatial variability.

Some Sensitivity Studies

It is natural to ponder upon the performance and reliability of the developed algorithm. Is there any norm to evaluate the algorithm? Or even if norms exist, is the algorithm sensitive to extreme cases? We performed a number of sensitivity studies to ascertain how robust is the developed code for simultaneous inversion of porosity and permeability.

- **Sensitivity to initial porosity/permeability fields.**

  The dynamic data integration algorithm relies on a minimization subproblem. In a gradient based minimization technique, initial model is an important factor for convergence. Thus, in our data integration problem porosity and permeability fields could as well be vital in the convergence of the algorithm. In order to illustrate the sensitivity of the inversion response to initial fields, we performed a number of exercises almost exactly similar to Example 1 Run 1 inversion but starting from different initial fields. The responses of the sensitivity exercise with different initial fields are tabulated in Table 1. Also shown in the table are the performance of Example 1 Run 1 for the purpose of comparison.

  The inverted models from the three sensitivity runs are shown in Figures 39, 40, and 41, respectively. The spatially connected high porosity/permeability bands connecting W2 and W3 are evident in all the inverted models except for the last one where the initial porosity and permeability fields are 0.4 and 6.0, respectively. Interestingly looking at the objective function values of the inversion processes in Table 1, we find that the last run has the best average pressure match.

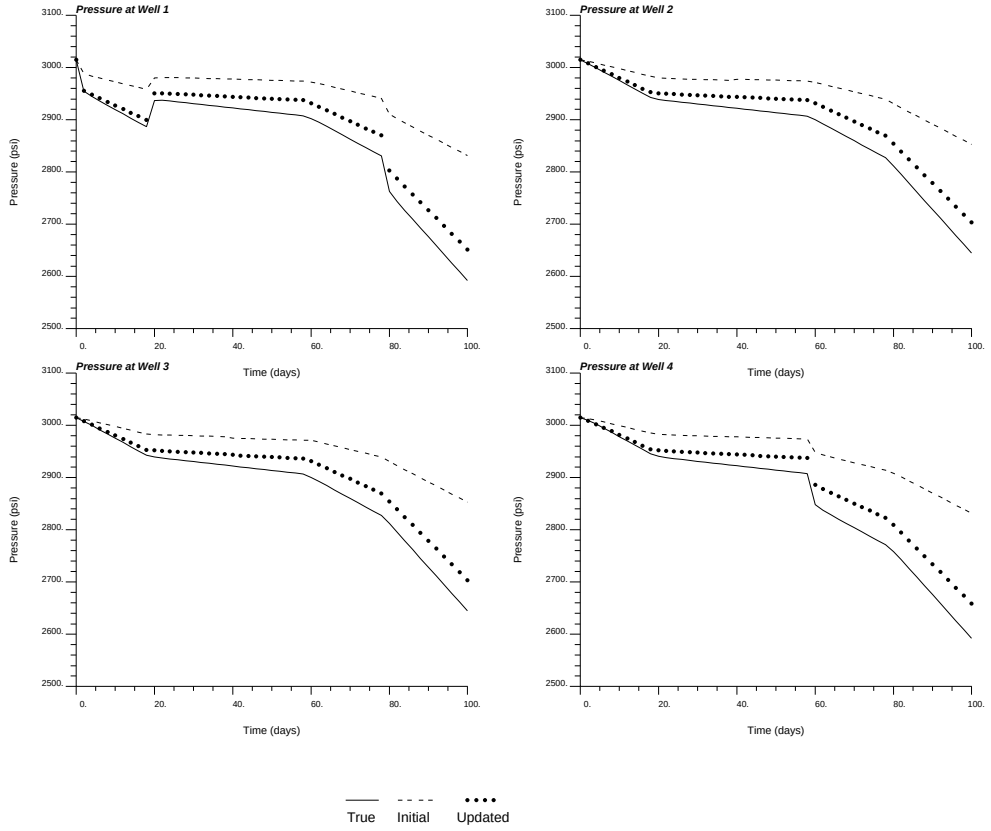

Figure 32: The pressure responses computed from intial (dashed lines) and updated (bullets) porosity and permeability fields with the true data (solid lines) : Example 1 Run 4.

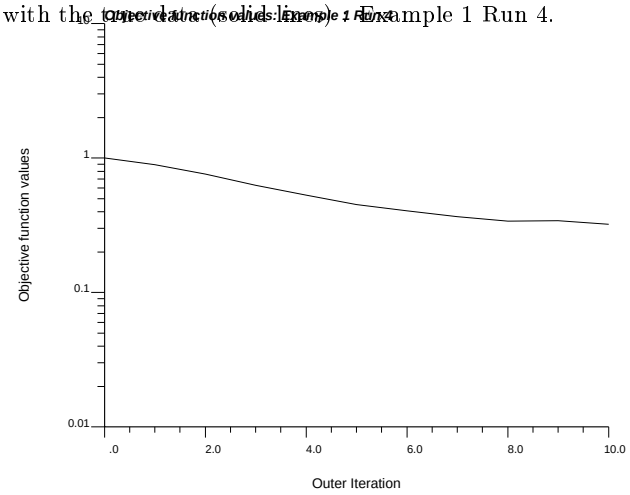

Figure 33: Objective function values of the simultaneous inversion process : Example 1 Run 4.

S. No.	**Initial** ϕ p.u.	**Initial** $\ln(k)$ ln(mD)	**Avg Mismatch** psi (L^2 norm)	**Outer Iter**	**CPU Time** sec
1	0.2	1.0	5.82	9	37
2	0.2	3.15	4.38	16	76
3	0.2	6.0	4.18	18	75
Ex 1 Run 1	0.4	3.15	4.1	17	75

Table 1: Sensitivity of simultaneous inversion to initial porosity and permeability fields

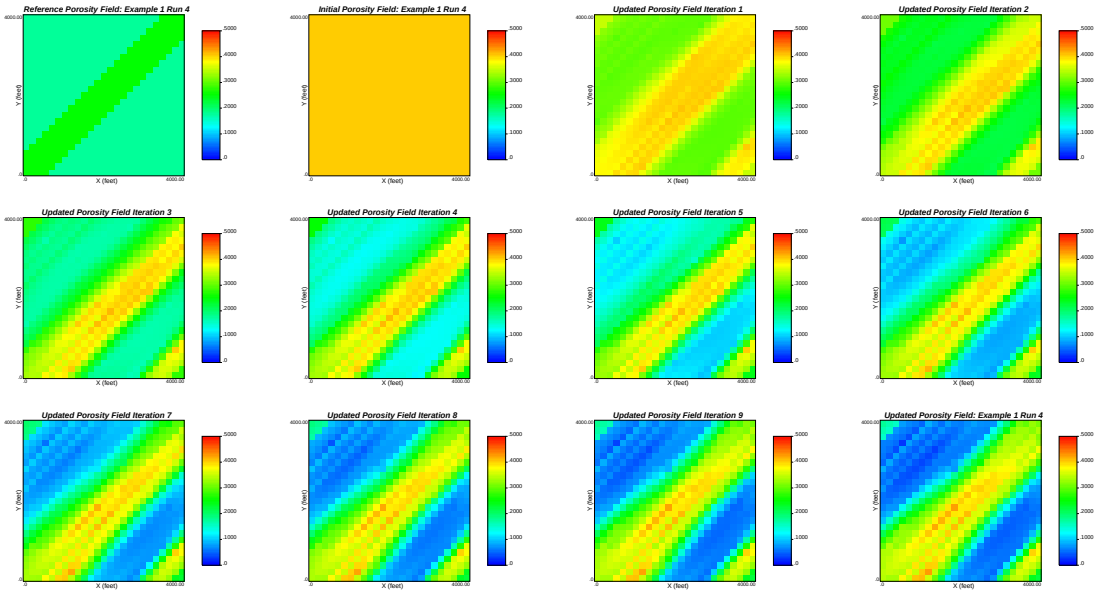

Figure 34: Updated porosity fields at each iteration of the simultaneous inversion process : Example 1 Run 4.

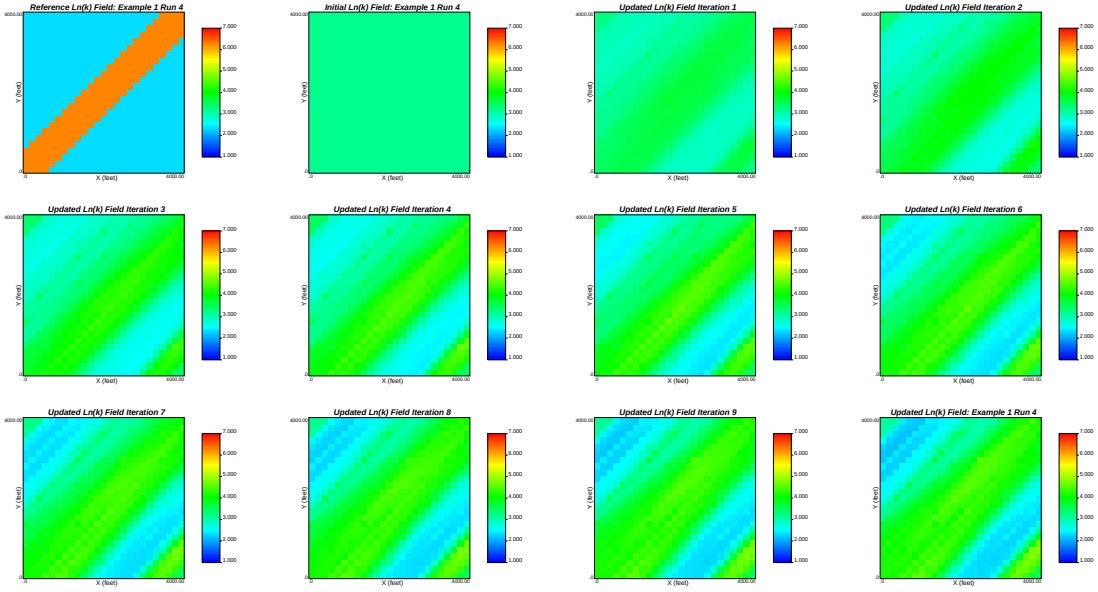

Figure 35: Updated Ln(k) fields at each iteration of the simultaneous inversion process : Example 1 Run 4.

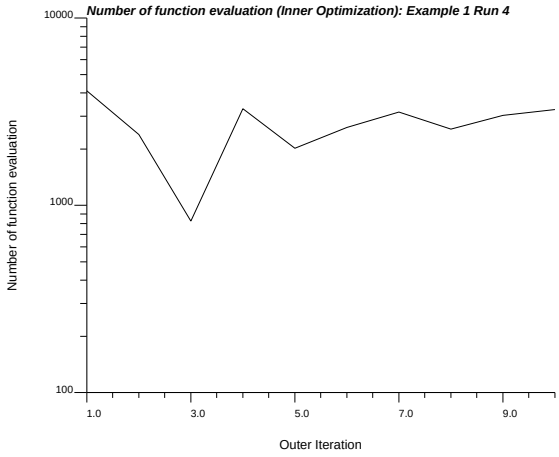

Figure 36: Number of function evaluation in the inner optimization loop for each outer iteration: Example 1 Run 4.

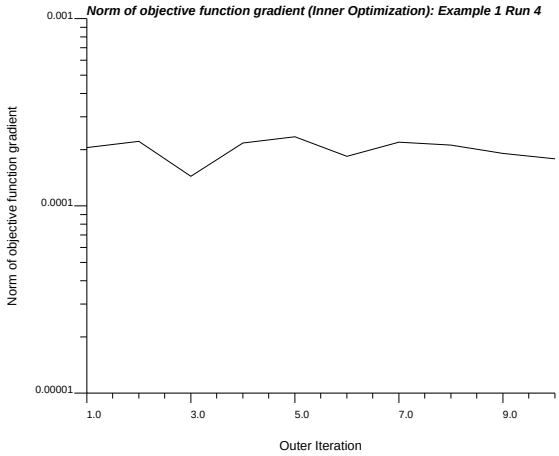

Figure 37: Norm of objective function gradient in the inner optimization loop at each outer iteration: Example 1 Run 4.

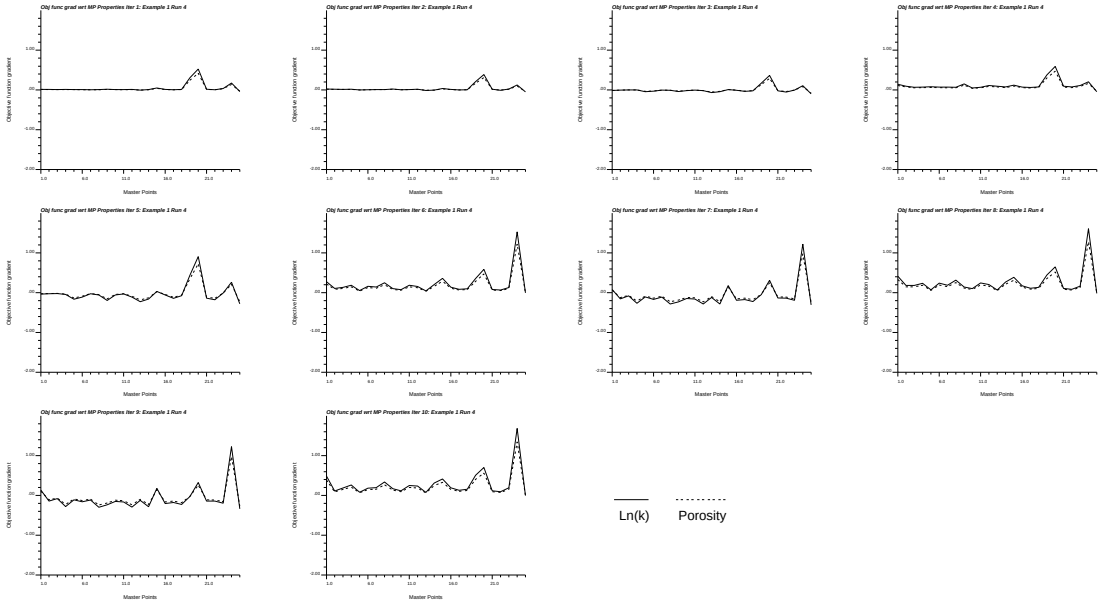

Figure 38: Gradient of the objective function with respect to Master Point permeability (solid lines) and porosity (dashed lines) at each outer iteration: Example 1 Run 4.

From the sensitivity exercise, it can be said that the algorithm has reasonable robustness feature with respect to the initial fields. However, the fact that there is no optimality criteria for global minima resounds its importance again. Some initial fields will fare better than others. Also, this sensitivity study reveals that looking only at the pressure match might not be a good rationale. Perhaps a regularization method with a model mismatch term will be even more effective criteria. Notwithstanding the fact that such regularization will also improve the stability of the algorithm.

- **Sensitivity to number of Master Points.**

  Master points are the cells of the model where porosity and permeability values are iteratively updated in order to minimize the pressure mismatch. Determinacy of an inversion problem could strongly depend on the relative amount of data and unknown parameters involved. Thus, number of Master Points could be an important element in the solution of the data integration algorithm.

  In order to illustrate the sensitivity of the inversion response to number of Master Points, a number of exercises almost with the specification as that in Example 1 Run 1 inversion is performed with varying number of Master Points. The number of Master Points are varied from 2×2 (=4) to 7×7 (=49). The responses of the sensitivity exercise with different number of Master Points are tabulated in Table 2. Also shown in the table are the performance of Example 1 Run 1 for the purpose of comparison.

  The inverted models from these sensitivity runs are shown in Figures 42, 43, 44, 45, and 46, respectively. The spatially connected high porosity/permeability bands connecting W2 and W3 are evident in all the inverted models. The objective function values of the inversion processes in Table 2 are reasonably good and ranges from 2.2 to 4.7 in L^2 norm sense.

  Envisaging the inverted models and the performance of the inversion process, increasing the number of Master Points may not improve the inversion pressure match. Having too few or too many Master Points might not be able to capture the major features as can be seen from

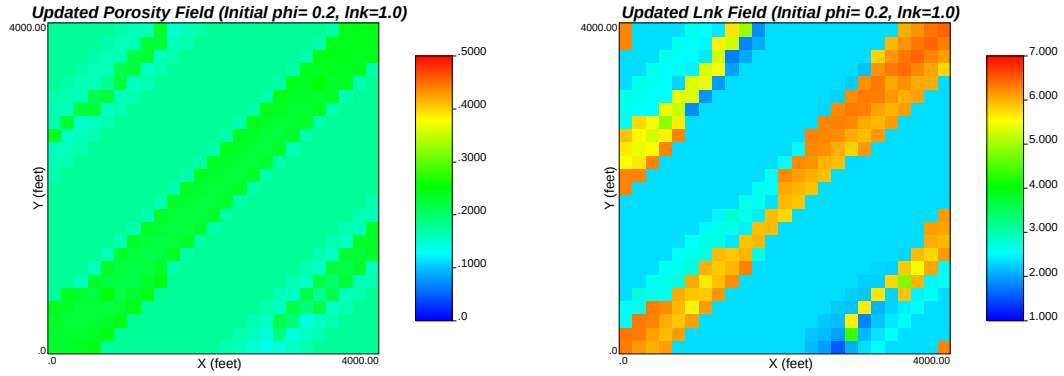

Figure 39: Updated porosity and permeability fields honoring production data, local hard data, global distribution and prior variography information using initial $\phi = 0.2$ and $\ln(k) = 1.0\,\ln(\text{mD})$.

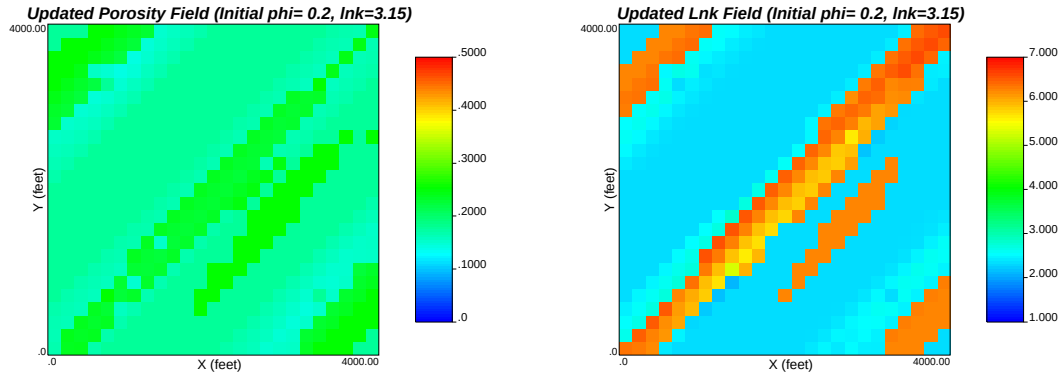

Figure 40: Updated porosity and permeability fields honoring production data, local hard data, global distribution and prior variography information using initial $\phi = 0.2$ and $\ln(k) = 3.15\,\ln(\text{mD})$.

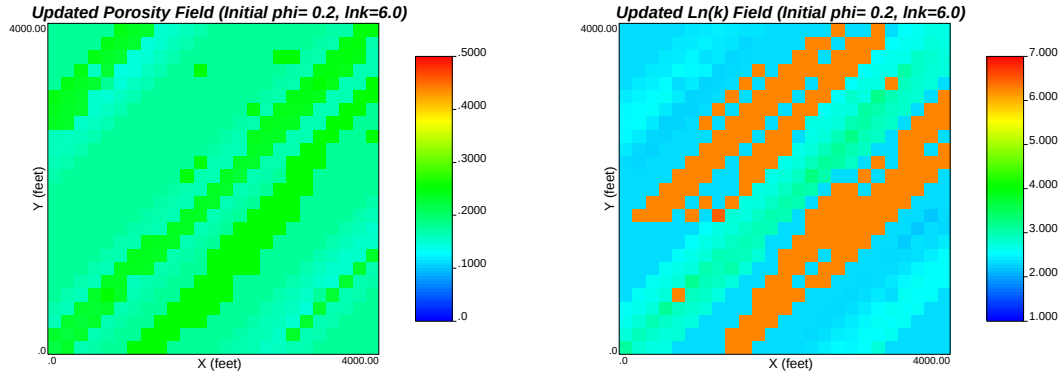

Figure 41: Updated porosity and permeability fields honoring production data, local hard data, global distribution and prior variography information using initial $\phi = 0.2$ and $\ln(k) = 6.0\,\ln(\text{mD})$. (Poor model)

S. No.	No. of Master Points X - Y	Avg Mismatch psi (L^2 norm)	Outer Iteration	CPU Time sec
1	2 - 2	3.01	15	15
2	3 - 3	2.24	12	20
3	4 - 4	4.52	12	35
4	6 - 6	3.22	18	92
5	7 - 7	4.65	10	112
Ex 1 Run 1	5 - 5	4.1	17	75

Table 2: Sensitivity of simultaneous inversion to number of Master Points

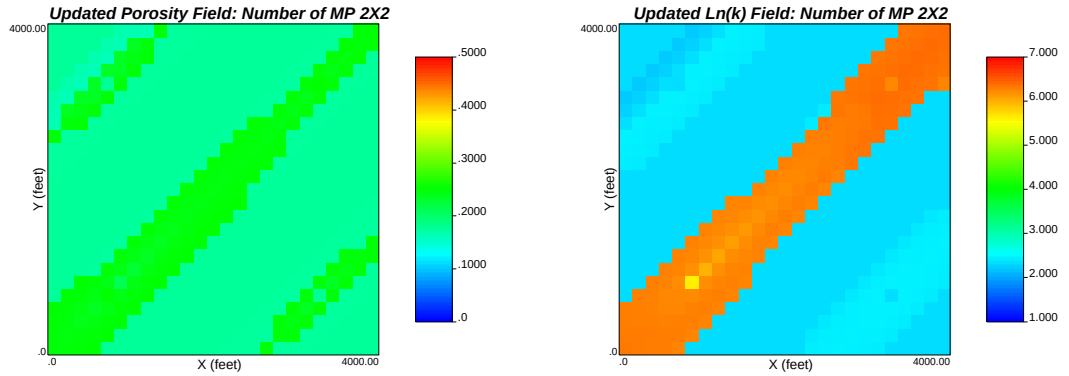

Figure 42: Updated porosity and permeability fields honoring production data, local hard data, global distribution and prior variography information using 2 × 2 Master Points.

this exercise. In case of 3 × 3 Master Points, although the mismatch norm is low (2.24), the inverted models have not captured the major features well relatively. It should be noted that as the number of Master Points increases, it becomes more computation intensive thus increasing the execution time.

- **Sensitivity to updating of Master Point locations.**

  Previous section dealt with the number of Master Points. It is conjectured that updating or changing the locations of the Master Points has a significant effect in the inversion process. The reason for such impact is that the inner optimization is actually implemented to find a minima. It cannot guarantee convergence to the global minima. In case of a situation where we are stuck with a local minima, it might be possible to shift away from the local minima to elsewhere in the feasible space by changing the locations of the Master Points.

  For investigating the sensitivity of the inversion response to location of Master Points, a number of exercises almost with the specification as that in Example 1 Run 1 inversion is performed with updating the Master Points after every few outer iterations. The frequency of updating of Master Point locations are varied from 1 to 10. The responses of the sensitivity exercise with different updating frequency are tabulated in Table 3. Also shown in the table are the performance of Example 1 Run 1 for the purpose of comparison. It should be noted that 5 × 5 (=25) Master Points are used in Example 1 Run 1 for the inversion.

  The inverted models from these sensitivity runs are shown in Figures 47, 48, 49, 50, 51 and 52, respectively. Inverted models are almost exactly similar in appearance. The objective function values of the inversion processes in Table 3 varies from about 1.6 to 8.3 in L^2 norm sense. Evidently, frequency of updating Master Point locations affects the number of outer iterations required to have the minimum mismatch shown in Table 3. However, it appears that location

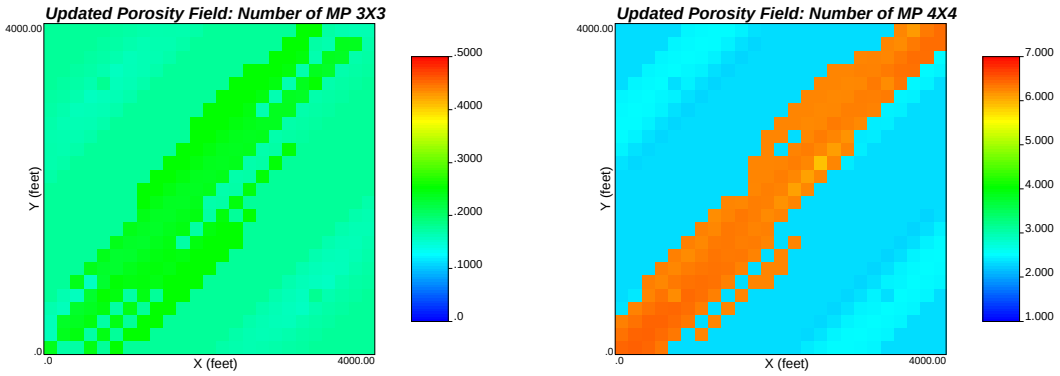

Figure 43: Updated porosity and permeability fields honoring production data, local hard data, global distribution and prior variography information using 3 × 3 Master Points.

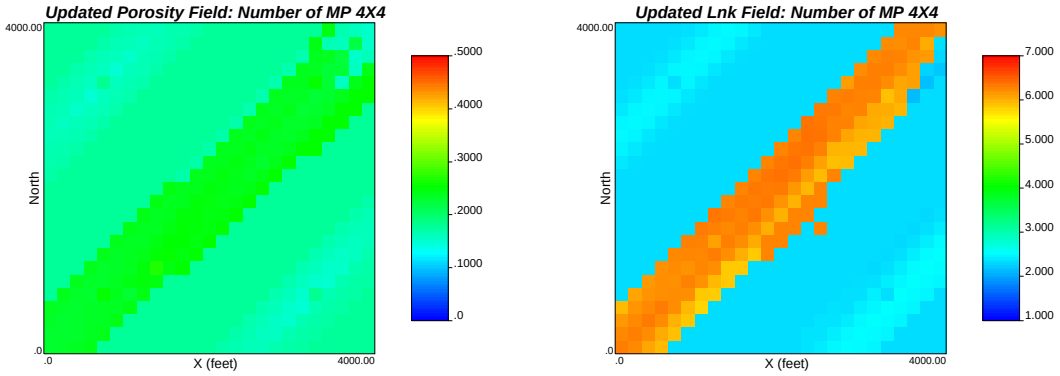

Figure 44: Updated porosity and permeability fields honoring production data, local hard data, global distribution and prior variography information using 4 × 4 Master Points.

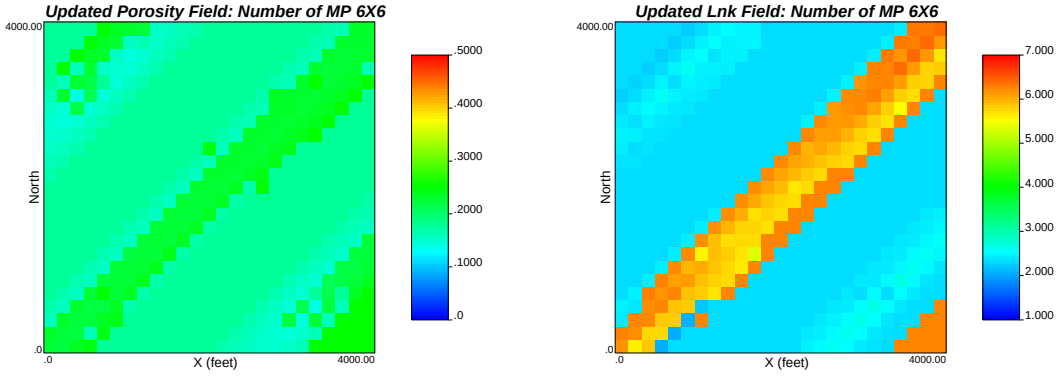

Figure 45: Updated porosity and permeability fields honoring production data, local hard data, global distribution and prior variography information using 6 × 6 Master Points.

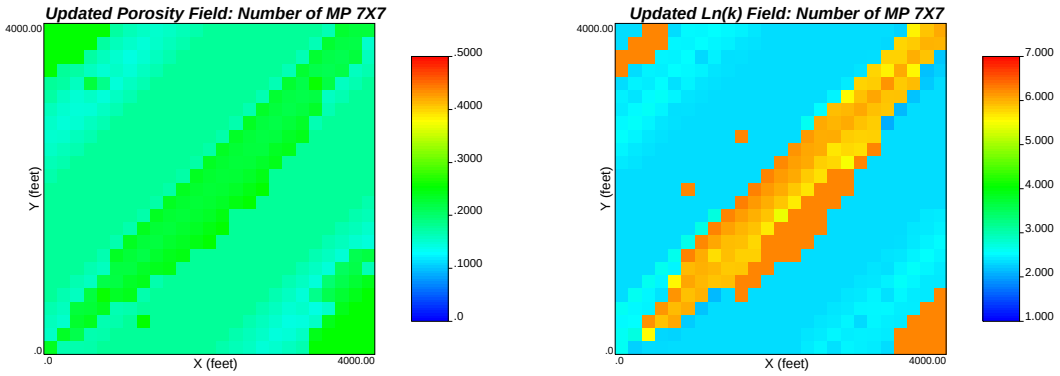

Figure 46: Updated porosity and permeability fields honoring production data, local hard data, global distribution and prior variography information using 7 × 7 Master Points.

S. No.	**Updating Freq**	**Avg Mismatch** psi (L^2 norm)	**Outer Iteration**	**CPU Time** sec
1	1	6.30	8	46
2	2	6.26	13	64
3	3	1.62	15	70
4	4	7.35	16	72
5	8	8.27	16	74
6	10	4.45	9	40
Ex 1 Run 1	5	4.1	17	75

Table 3: Sensitivity of simultaneous inversion to updating frequency of Master Point locations

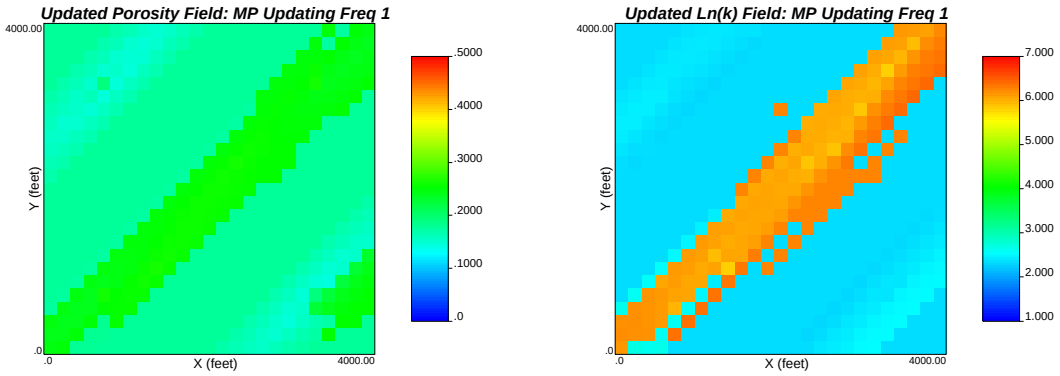

Figure 47: Updated porosity and permeability fields honoring production data, local hard data, global distribution and prior variography information updating Master Point locations every outer iteration.

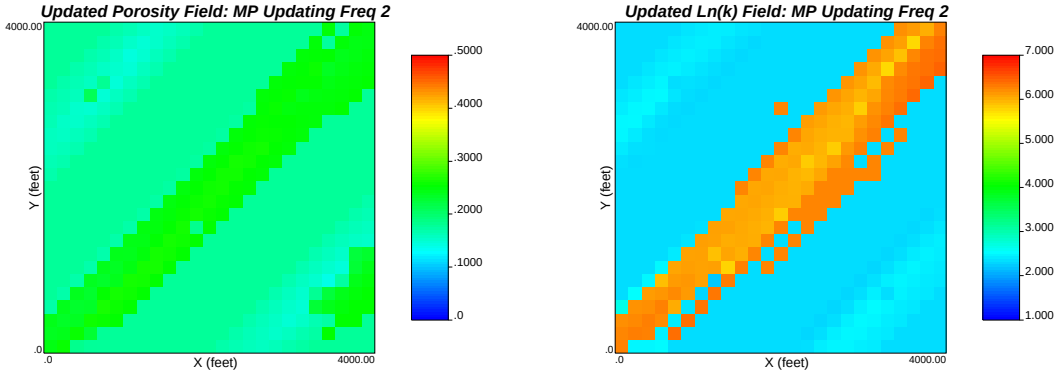

Figure 48: Updated porosity and permeability fields honoring production data, local hard data, global distribution and prior variography information updating Master Point locations every 2 outer iterations.

updating did not have the expected impact on convergence to global minima.

- **Sensitivity to prior variogram information.**

  Prior variogram information is an important factor in a good reservoir characterization study. From the first exercise in the previous section, it was evident that variography has a significant impact on the inverted models. However, the right variography is extremely difficult to gather if not impossible. So a sensitivity study of the models to variography could ascertain how well the algorithm could resolve or characterize the reservoir parameters.

  In order to illustrate the sensitivity of the inversion response to variography, a number of exercises almost with the specification as that in Example 1 Run 1 inversion is performed using different variogram information. The variogram information used for the sensitivity studies are tabulated in Table 4. Variogram anisotropy was changed from a ratio of about 8:1 to 4:1. Anisotropy angle was varied from 20^o to 70^o. The responses of the sensitivity exercise with different prior variography information are tabulated in Table 5. Also shown in the table are the performance of Example 1 Run 1 for the purpose of comparison.

  The inverted models from these sensitivity runs are shown in Figures 53, 54, 55, and 56, respectively. Inverted models are almost exactly similar in appearance. The objective function

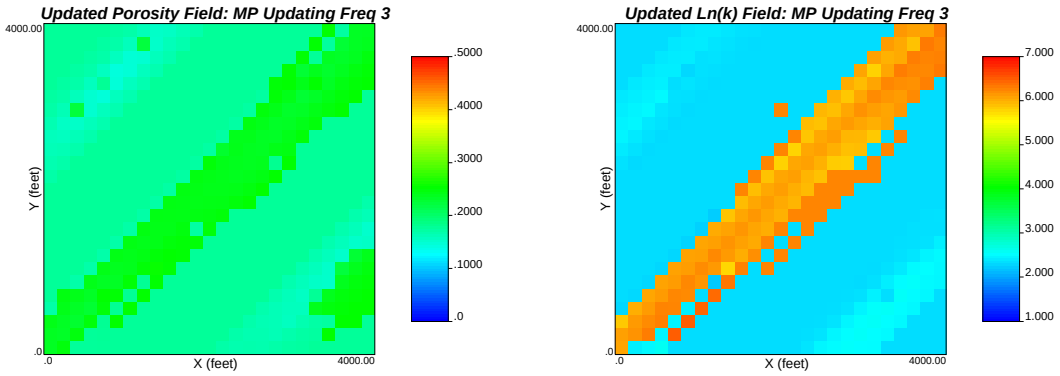

Figure 49: Updated porosity and permeability fields honoring production data, local hard data, global distribution and prior variography information updating Master Point locations every 3 outer iterations.

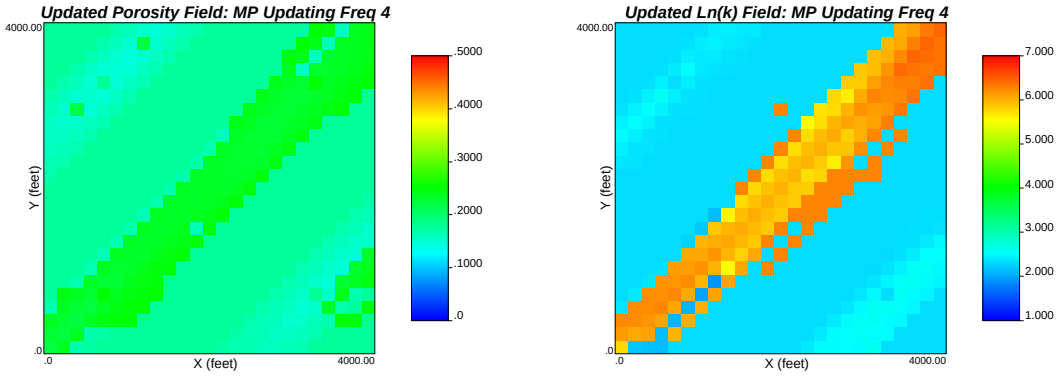

Figure 50: Updated porosity and permeability fields honoring production data, local hard data, global distribution and prior variography information updating Master Point locations every 4 outer iterations.

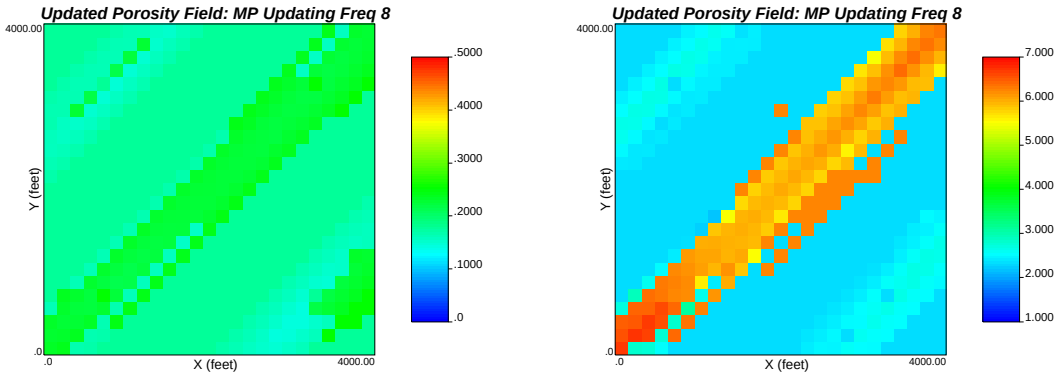

Figure 51: Updated porosity and permeability fields honoring production data, local hard data, global distribution and prior variography information updating Master Point locations every 8 outer iterations.

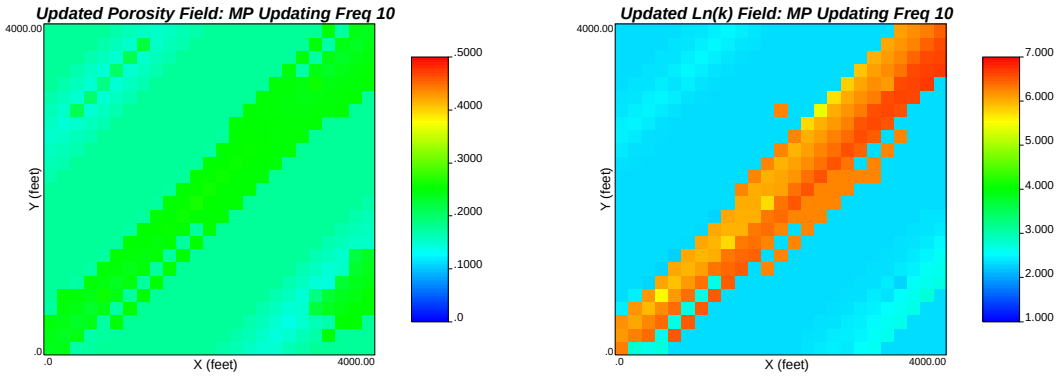

Figure 52: Updated porosity and permeability fields honoring production data, local hard data, global distribution and prior variography information updating Master Point locations every 10 outer iterations.

S. No.	$\ln(k)$ **Range** X - Y (ft)	$\ln(k)$ **Angle** (^{o})	ϕ **Range** X - Y (ft)	ϕ **Angle** (^{o})
1	8100 - 1000	20	8000 - 1100	20
2	8100 - 1000	70	8000 - 1100	70
3	6100 - 1000	45	6000 - 1100	45
4	4100 - 1000	45	4000 - 1100	45
Ex 1 Run 1	8100 - 1000	45	8000 - 1100	45

Table 4: Prior variogram information used in sensitivity exercise.

S. No.	**Avg Mismatch** psi (L^2 norm)	**Outer Iteration**	**CPU Time** sec
1	2.80	20	89
2	2.35	12	63
3	3.40	14	66
4	2.23	16	76
Ex 1 Run 1	4.1	17	75

Table 5: Response of sensitivity exercise to prior variography information.

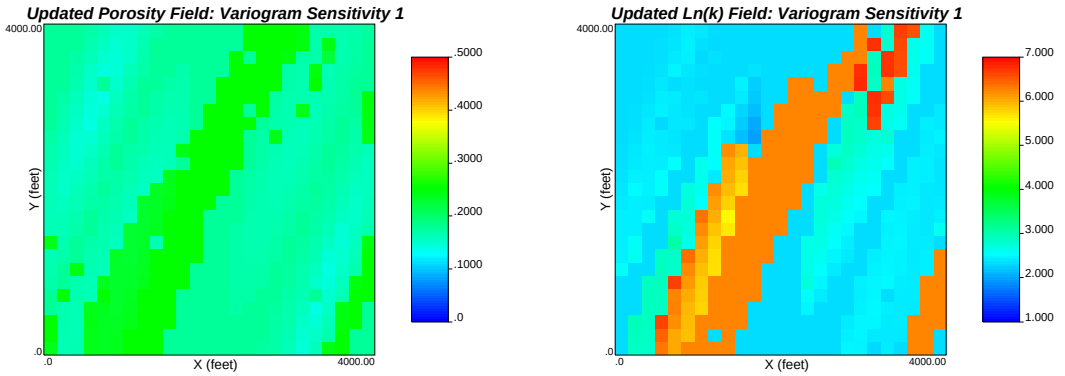

Figure 53: Updated porosity and permeability fields honoring production data, local hard data, global distribution and prior variography information using variogram set 1 in Table 4.

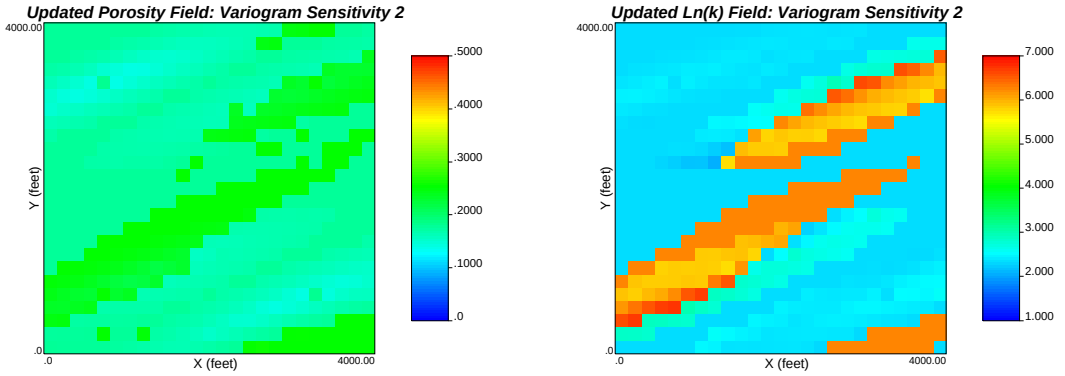

Figure 54: Updated porosity and permeability fields honoring production data, local hard data, global distribution and prior variography information using variogram set 2 in Table 4.

values of the inversion processes in Table 5 varies from about 2.2 to 4.1 in L^2 norm sense. These are reasonably good pressure match values.

- **Sensitivity to inner optimization parameters.**

  In the inner optimization module, the object is to search for a primal local minima under bound constraints of the ϕ, $\ln(k)$ correction values. An approximate subproblem of our original data integration problem is formulated for the minimization. Questions occur: how good is the solution of this optimization subproblem? Is there a possibility of data over-fitting in the subproblem? Some qualitative answer to these legitimate questions can be scrounged by a sensitivity study of the inversion algorithm to the inner optimization parameters. We can relax the termination criteria in the minimization problem and analyze the final inverted models and the number of function evaluations to arrive at these models.

  In order to demonstrate the sensitivity of the inversion response to inner optimization parameters, a number of exercises almost with the specification as that in Example 1 Run 1 inversion is performed by varying the tolerance values for objective function convergence and norm of the gradient. The inner optimization parameters used for the sensitivity studies are tabulated in Table 6. The responses of the sensitivity exercise with different inner optimization parameters are tabulated in Table 7. Also shown in the table are the performance of Example 1 Run

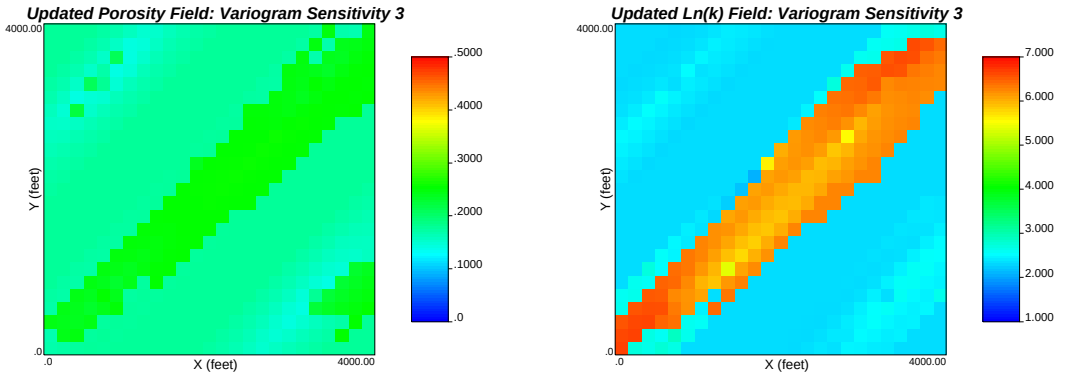

Figure 55: Updated porosity and permeability fields honoring production data, local hard data, global distribution and prior variography information using variogram set 3 in Table 4.

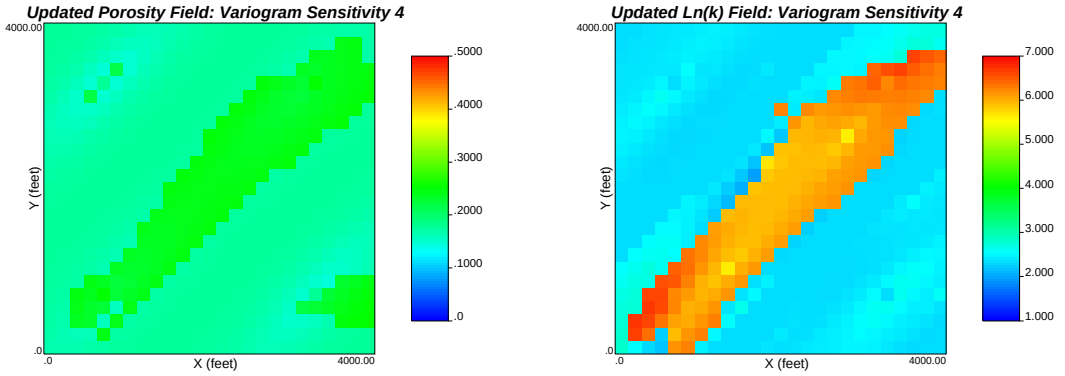

Figure 56: Updated porosity and permeability fields honoring production data, local hard data, global distribution and prior variography information using variogram set 4 in Table 4.

S. No.	Grad Norm Tol	Obj Func Tol	Obj Func Conv No.
1	5.0×10^{-4}	1.0×10^{-5}	40
2	5.0×10^{-4}	1.0×10^{-5}	10
3	5.0×10^{-5}	1.0×10^{-5}	10
4	5.0×10^{-4}	1.0×10^{-4}	40
Ex 1 Run 1	5.0×10^{-5}	1.0×10^{-5}	40

Table 6: Inner optimization parameters used in sensitivity exercise.

S. No.	Avg Mismatch psi (L^2 norm)	Outer Iteration	CPU Time sec
1	2.51	18	79
2	6.93	14	50
3	3.72	7	32
4	3.35	10	36
Ex 1 Run 1	4.1	17	75

Table 7: Response of sensitivity exercise to inner optimization parameters.

1 for the purpose of comparison.

Inverted models (not shown here) capture major heterogeneity features of the reference field. However, the objective function values of the inversion processes in Table 7 varies significantly from about 2.5 to 6.9 in L^2 norm sense. Number of function evaluation in the inner optimization loop for each outer iteration are shown in Figures 57, 59, 61, and 63, respectively for the corresponding optimization parameters. Norm of objective function gradient in the inner optimization loop at each outer iteration is shown in Figures 58, 60, 62, and 64, respectively. It could be observed from these figures that when the tolerance for gradient comparison is 5×10^{-4}, the number of function and gradient evaluation remains at the assigned minimum (here 50) after first few outer iterations. However when this value is fixed at 5×10^{-5} (more stringent tolerance), this termination criteria is not met and the number of function evaluation is much higher (over 1000). Minimum number of convergence of subsequent iterations has minimal effect on the inversion process, as can be seen by comparing the gradient norm curves in Set 1 with Set 2, and Set 3 with Set 4.

Some Implementation Issues

Issue 1: **Implementation issue regarding propagation of optimal corrections.**

In the algorithm optimal corrections from the inner optimization at Master Point locations are propagated onto the entire field by kriging. For ϕ corrections $\Delta_{\phi,i}$ we use kriging equation (Equation 1), whereas for $y = \ln(k)$ corrections $\Delta_{y,i}$ we employ the collocated cokriging equation (Equation 2). The correction propagation equations are shown in Equations 11 and 12 for ϕ and $\ln(k)$ respectively.

$$\Delta_{\phi,i} = \sum_{j=1}^{n_{mp}} \tau_{i,j}^{\phi} \Delta_{\phi,j} \tag{11}$$

$$\Delta_{y,i} = \sum_{j=1}^{n_{mp}} \tau_{i,j}^{y} \Delta_{y,j} + \xi_i \Delta_{\phi,i} \tag{12}$$

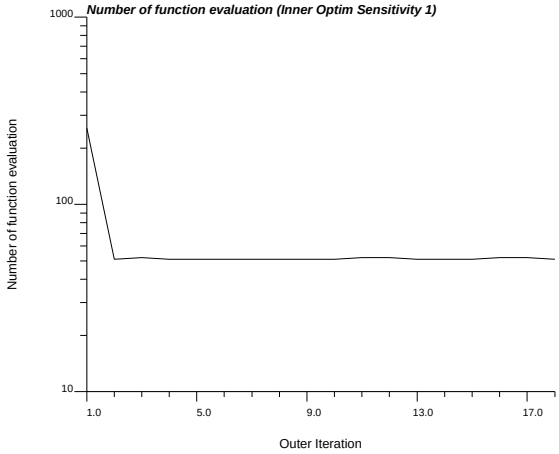

Figure 57: Number of function evaluation in the inner optimization loop for each outer iteration: inner optimization sensitivity 1.

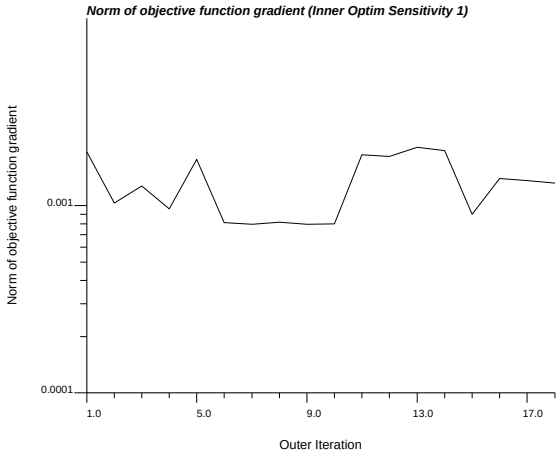

Figure 58: Norm of objective function gradient in the inner optimization loop at each outer iteration: inner optimization sensitivity 1.

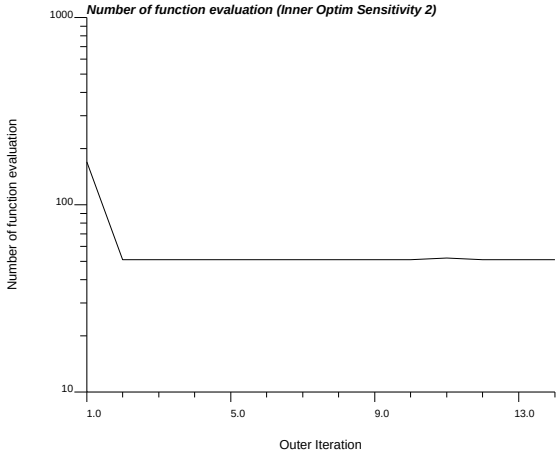

Figure 59: Number of function evaluation in the inner optimization loop for each outer iteration: inner optimization sensitivity 2.

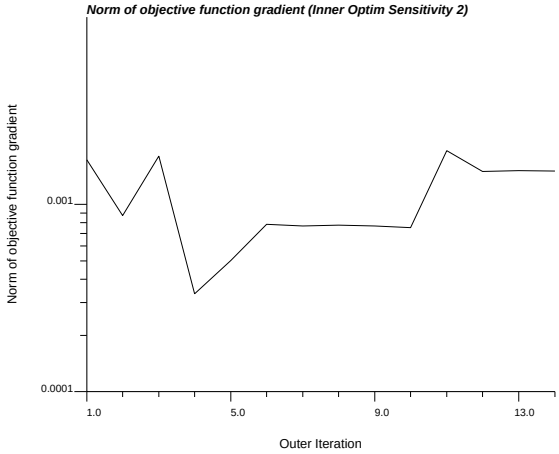

Figure 60: Norm of objective function gradient in the inner optimization loop at each outer iteration: inner optimization sensitivity 2.

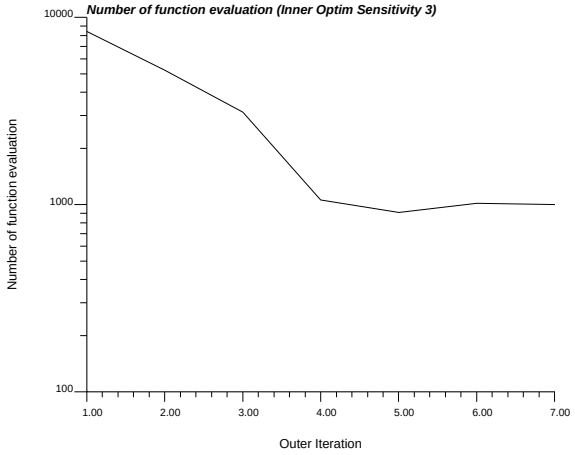

Figure 61: Number of function evaluation in the inner optimization loop for each outer iteration: inner optimization sensitivity 3.

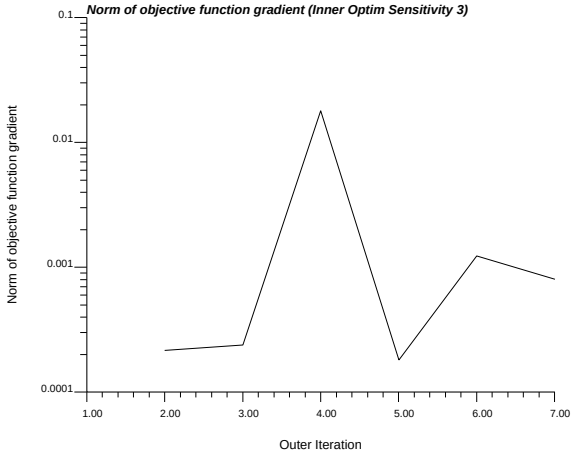

Figure 62: Norm of objective function gradient in the inner optimization loop at each outer iteration: inner optimization sensitivity 3.

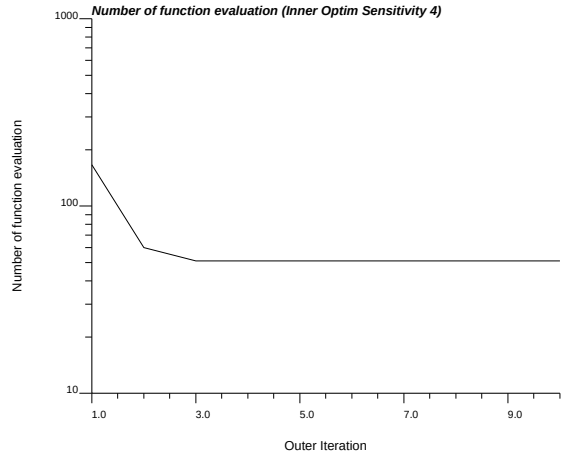

Figure 63: Number of function evaluation in the inner optimization loop for each outer iteration: inner optimization sensitivity 4.

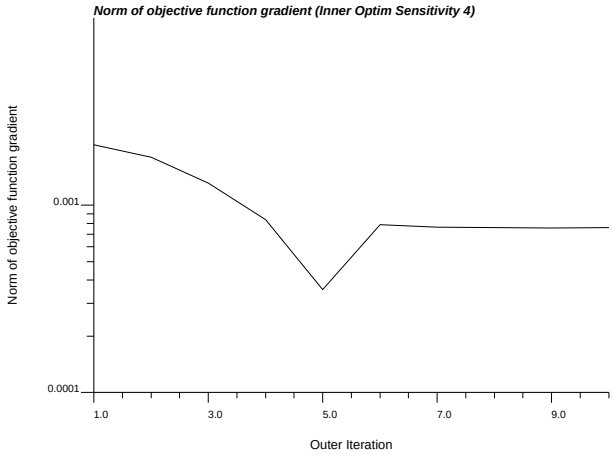

Figure 64: Norm of objective function gradient in the inner optimization loop at each outer iteration: inner optimization sensitivity 4.

The average corrections $\overline{\Delta}$ in the near-optimal region will assume trivial values (zero). However, at other points these may take non-trivial values. In the latter case, the above optimal correction equations are more appropriately modified to Equations 13 and 14 for ϕ and $\ln(k)$ respectively.

$$\Delta_{\phi,i} = \sum_{j=1}^{n_{mp}} \tau_{i,j}^{\phi} \Delta_{\phi,j} + \left(1 - \sum_{j=1}^{n_{mp}} \tau_{i,j}^{\phi}\right) \overline{\Delta_{\phi}} \tag{13}$$

$$\Delta_{y,i} = \sum_{j=1}^{n_{mp}} \tau_{i,j}^{y} \Delta_{y,j} + \xi_i(\Delta_{\phi,i} - \overline{\Delta_{\phi}}) + \left(1 - \sum_{j=1}^{n_{mp}} \tau_{i,j}^{y}\right) \overline{\Delta_{y}} \tag{14}$$

where $\overline{\Delta_{\phi}}$ and $\overline{\Delta_{y}}$ are average Δ_{ϕ} and Δ_{y}, respectively. For our convenience, we label the implementation using Equations 13 and 14 as 'Opt 1' and the other 'Opt 2'.

A geostatistician would discern the two implementations by the difference between simple kriging and and ordinary kriging. However, it was found that the performance of Implementation Opt 1 is better than Implementation Opt 2. It has been observed that it is more likely to get into degeneracy problems when using Implementation Opt 2. In fact, we employed Implementation Opt 1 for most inversion shown in this study. In order to illustrate the difference between the two implementation, we performed the Example 1 Run 1 inversion and compared the performance.

With Implementation Opt 2, the inverted models are obtained after 16 outer iterations (77 seconds in 733 MHz dual processor workstation). These inverted models are shown in Figure 65. The spatially connected high porosity/permeability bands connecting W2 and W3 are evident in the inverted models. However, the major features are not captured with as much details as it was obtained using Implementation Opt 1 in Example 1 Run 1. Figure 66 shows the pressure values at the four wells computed from the true (from reference), initial and final updated porosity and permeability fields. The objective function values of the inversion process is shown in Figure 67. Comparing the objective functions curves for the cases (Figures 5 and 67), it can be seen that Implementation Opt 1 is smoother than the other. Final average pressure mismatch (in L^2 norm sense) for 200 data in both the implementations is 4.13 psi. Updated porosity and permeability fields after each outer iteration of the inversion method are shown in Figures 68 and 69. Number of function evaluation in the inner optimization loop for each outer iteration are shown in Figure 70. Norm of objective function gradient in the inner optimization loop at each outer iteration is shown in Figure 71. The gradient of the objective function at each outer iteration is shown in Figure 72. It should be noted that the scale of the objective function gradients at iterations 8 and 9 (shown in Figure 72) are from -2 to 10, while for other iterations it is -2 to 2. Sharp changes in the gradients indicate the possibility of getting into numerical problems when using Implementation Opt 2.

Discussion

The paper presented a newly developed algorithm for simultaneous inversion of porosity and permeability via collocated cokriging method. The implemented code has been demonstrated with some synthetic and realistic reservoir example. Some sensitivity studies have been performed to investigate how robust is the algorithm. Some implementation issues have been related in order to show what and how controls can we have in the inversion process. It can be remarked that results proves to be a positive and informative study. However, there are scopes of improvement in this area of research. Some facets of improvement would be to explore the optimization and search algorithm, incorporating compartmentalized reservoir concept into the algorithm, integrating for more complex reservoir scenarios.

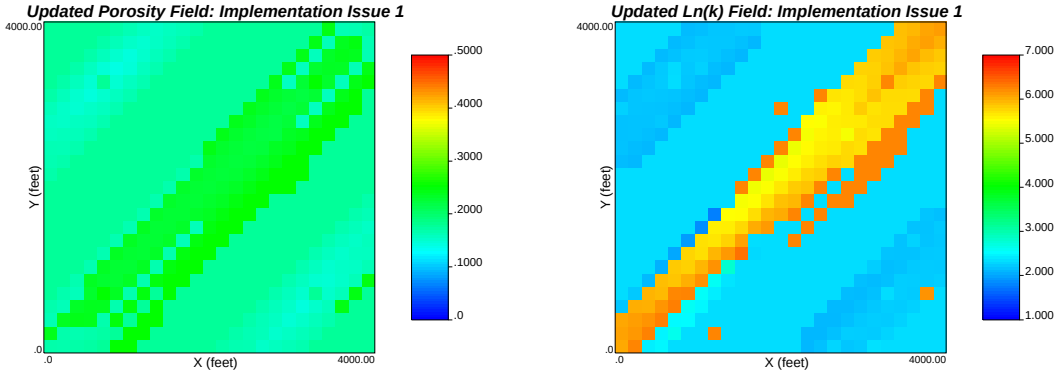

Figure 65: Updated porosity and permeability fields honoring production data, local hard data, global distribution and prior variography information : Implementation Issue 1 (same inversion exercise as in Example 1 Run 1).

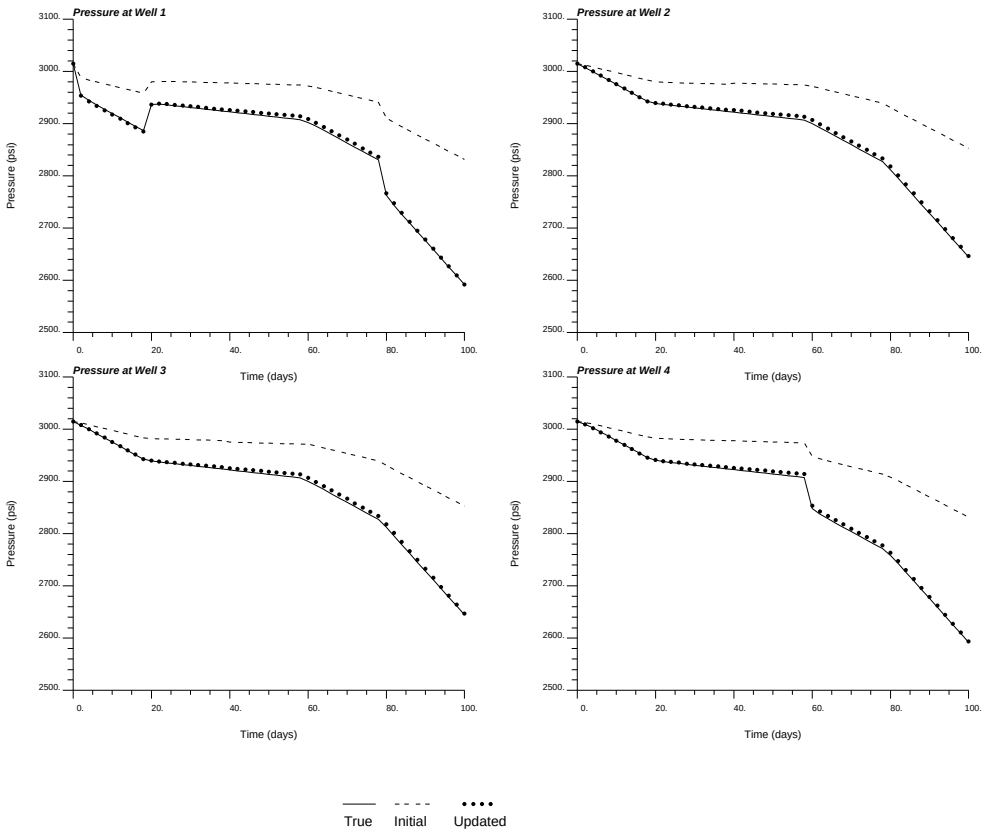

Figure 66: The pressure responses computed from intial (dashed lines) and updated (bullets) porosity and permeability fields with the true data (solid lines) : Implementation Issue 1 (same inversion exercise as in Example 1 Run 1).

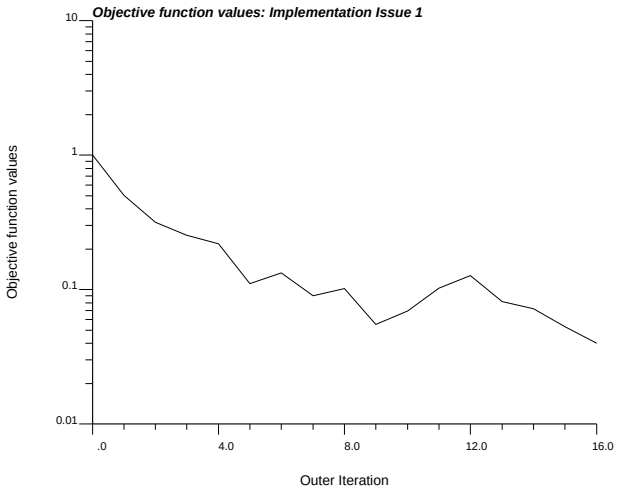

Figure 67: Objective function values of the simultaneous inversion process : Implementation Issue 1 (same inversion exercise as in Example 1 Run 1).

Some Suggested Areas of Improvement

Some suggested areas of improvement or future work on this topic would be the following.

- Stress should be given to implement a better or more robust optimization algorithm. Currently, work is being done in implementing better bound constrained optimization.
- Implementation of some global optimization modules could be considered.
- More realistic reservoir scenarios should be incorporated. Multiphase reservoir simulation option should be added into the integration algorithm. Extension to 3D case is virtually imminent.
- Compartmentalization of reservoirs based on stratigraphy or lithofacies could be looked into.

Appendix

```
            Parameters for SSCKPHI
            **********************

START OF PARAMETERS:
wd101201\well.dat             -file with local well conditioning phi,ln(k) data
1  2  4  0  5  0              -columns for X, Y coordinates, phi,ln(k) & error
4  4  4                       -num. of phi,ln(k) data & num. of wells with flow data
1                             -index for identifying desired histogram
wd101201\ref2dpk1012_1.dat    -file with phi/ln(k) histogram (scale of SSC model)
1  0  2  0                    -columns for phi,permeability and weight
3.0 10. 3.0 10.               -tail interpolation parameters for phi, ln(k)
3.75   1.75                   -mean and variance of ln(k) distribution
0.2    0.025                  -mean and variance of phi distribution
wd101201\wellpara2.dat        -file with reservoir and well data
wd101201\flowrate2.dat        -file with input flow rate and time step data
wd101201\mwspf1012_r2.out     -file with input pressure data
wd101201\boundary.dat         -file with boundary conditions
wd101201\pinit.dat            -file with initial pressure for the entire field
wd101201\seed1012_1.dat       -file with input realizations
1  2                          -number for phi and perm
1  1  1                       -number of total, start and end realizations
0  1.0e21 -9.0  1.0e21        -trimming limits for missing values
```

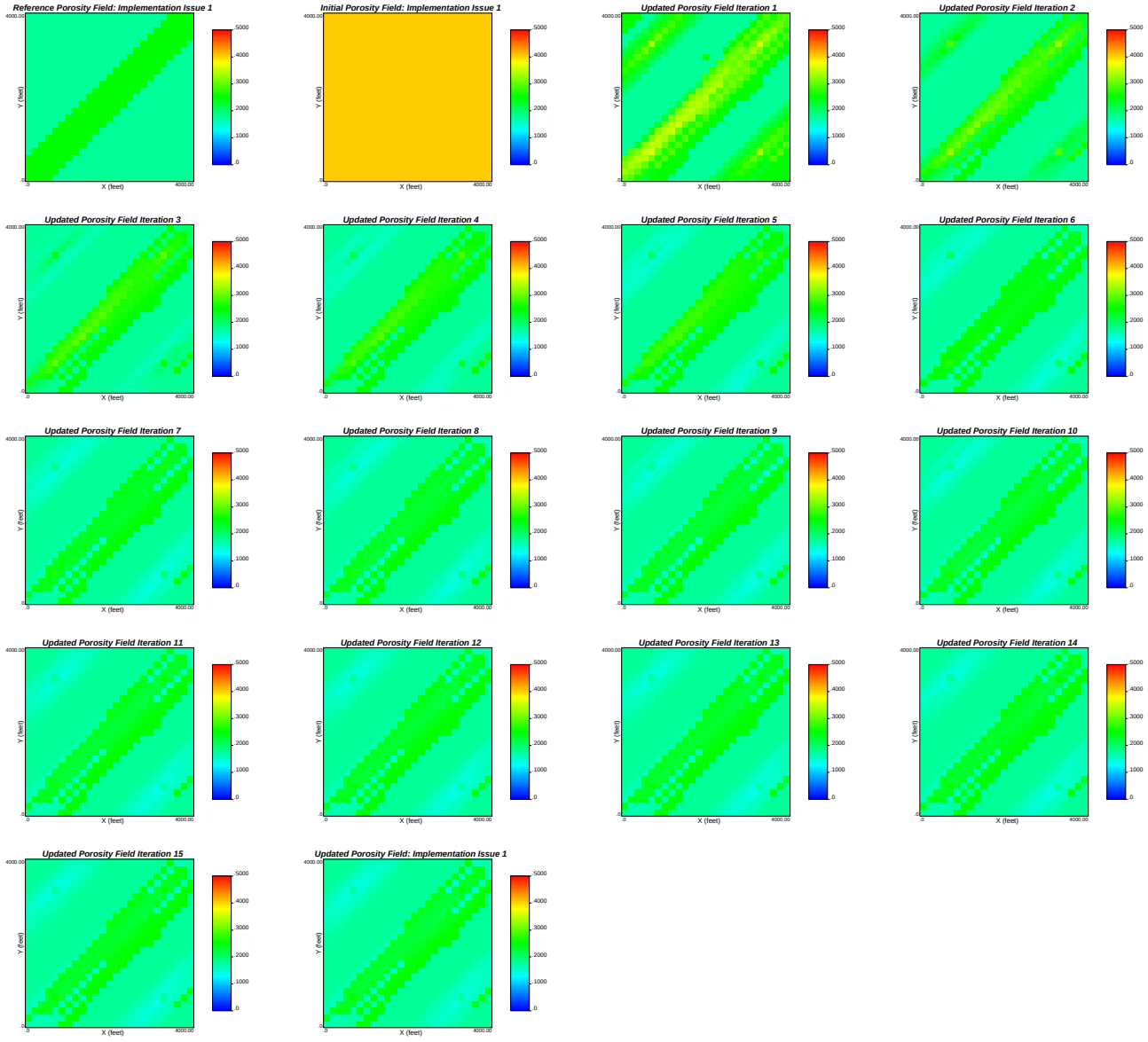

Figure 68: Updated porosity fields at each iteration of the simultaneous inversion process : Implementation Issue 1 (same inversion exercise as in Example 1 Run 1).

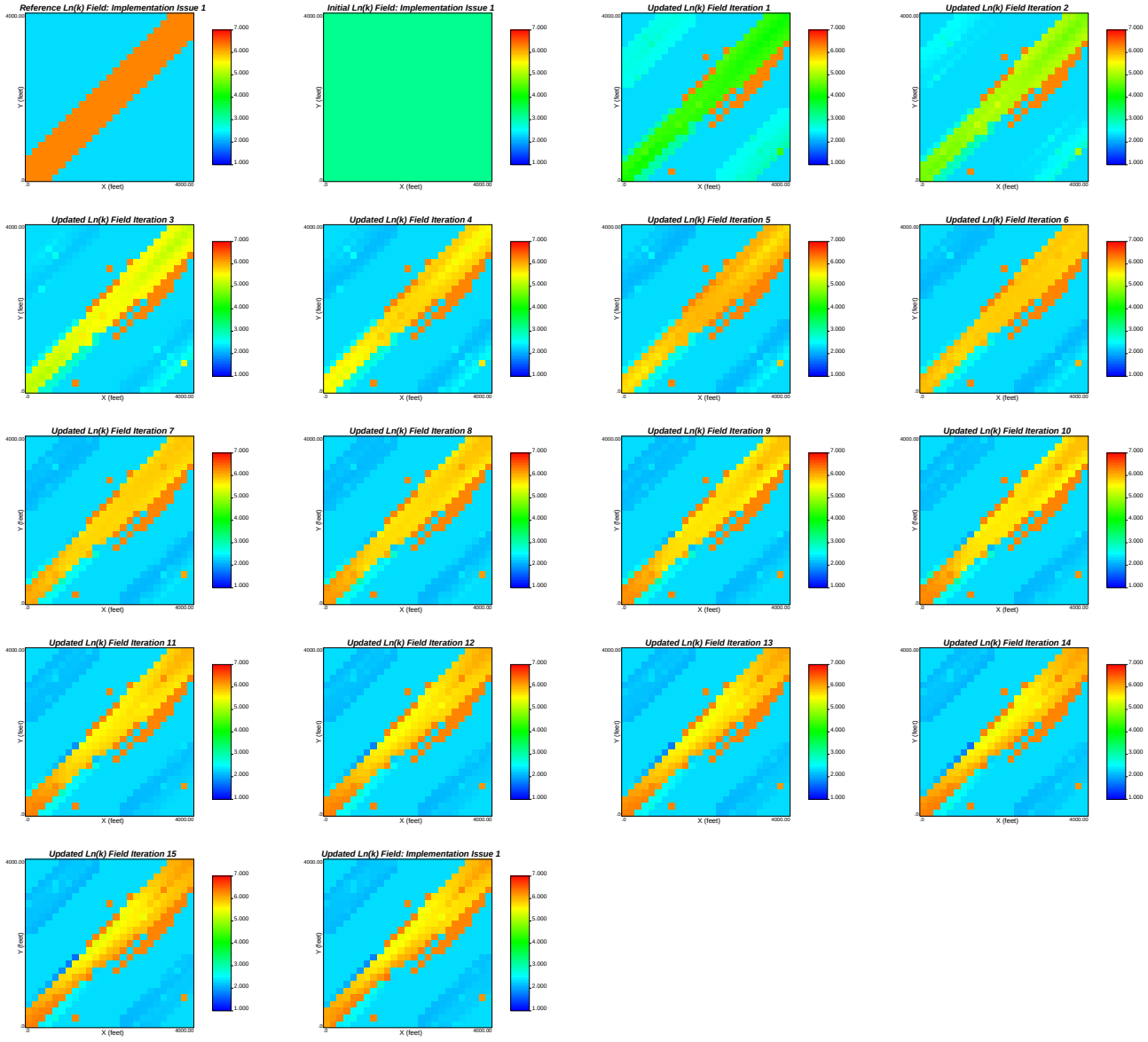

Figure 69: Updated Ln(k) fields at each iteration of the simultaneous inversion process : Implementation Issue 1 (same inversion exercise as in Example 1 Run 1).

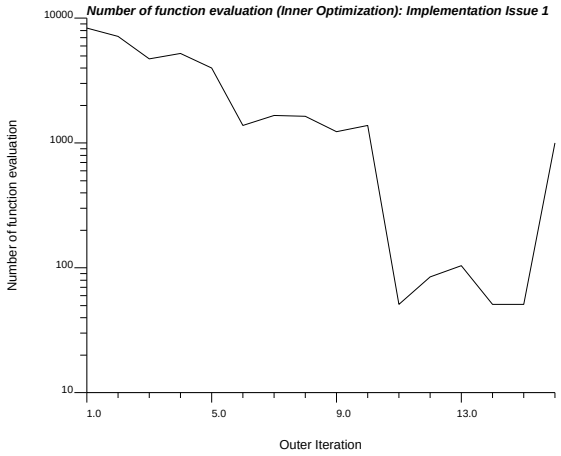

Figure 70: Number of function evaluation in the inner optimization loop for each outer iteration: Implementation Issue 1 (same inversion exercise as in Example 1 Run 1).

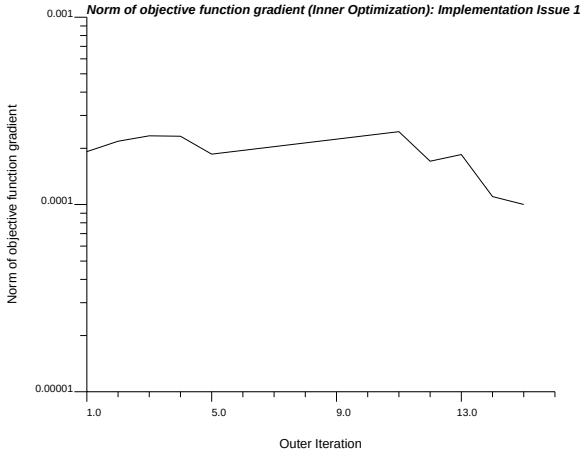

Figure 71: Norm of objective function gradient in the inner optimization loop at each outer iteration: Implementation Issue 1 (same inversion exercise as in Example 1 Run 1).

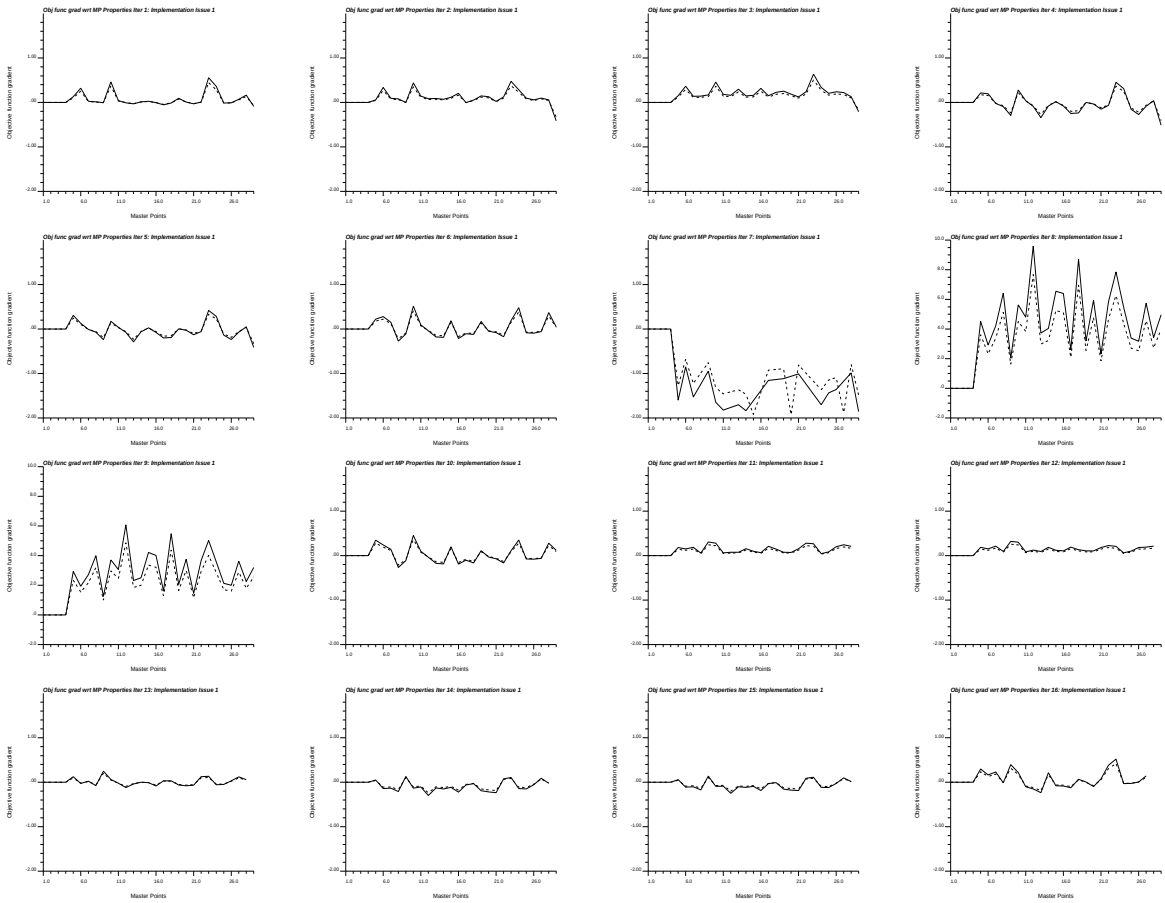

Figure 72: Gradient of the objective function with respect to Master Point permeability (solid lines) and porosity (dashed lines) at each outer iteration : Implementation Issue 1 (same inversion exercise as in Example 1 Run 1)

```
5                              -debugging level
wd101201\ssc1012_r2y.dbg       -file for debug output
wd101201\ssc1012_r2y.out       -file for output ln(k) realizations
wd101201\obj1012_r2y.out       -file for output objective function after each iter
wd101201\prm1012_r2y.out       -file for output matching of pressure responses
25  80.0  160.0                -X grid size: nx, xmn, xsiz
25  80.0  160.0                -Y grid size: ny, ymn, ysiz
45774                          -random number seed
5   5                          -number of master points in X and Y
5                              -number of outer iterations to update master points
1.0                            -factor for defining constraint interval for optim.
17  0.3   0.0001               -max num of outer iter, dumping para & min tol
50  5.e-5  5.e-5  1.e-5  40    -optimization parameters
3000.                          -search radius for kriging
1  16                          -min and max num. of samples for kriging
0                              -type of kriging (phi)
0.8                            -correlation coefficient of phi,ln(k)
1  0.05                        -nst, nugget effect (phi)
1  .95  45.0  8000.0 1100.0    -type, sill, azm, max range, min range
1  0.05                        -nst, nugget effect (perm)
1  .95  45.0  8100.0 1000.0    -type, sill, azm, max range, min range
```

Figure 73: Parameter file for the program, SSCKPHI: Example 1 Run1.

```
Well values for SSCKPHI Runs
 5
X
Y
Z
Porosity
Ln(k)
    720.000     3280.000        0.500        0.175        2.3026
    3280.000    3280.000        0.500        0.250        6.2146
    720.000     720.000         0.500        0.250        6.2146
    3280.000    720.000         0.500        0.175        2.3026
```

Figure 74: Hard well data required for runs in Example 1: Runs 1 and 3.

```
Data file with phi, k data
2
phi
ln(k)
   .2500       6.2146
   .2500       6.2146
   .2500       6.2146
   .2500       6.2146
   .1750       2.3026
          .
        .
        .
   .1750       2.3026
   .2500       6.2146
   .2500       6.2146
   .2500       6.2146
   .2500       6.2146
```

Figure 75: Global distribution data required for runs in Example 1: Runs 1 and 2.

```
4   0.2     100.0    0.2     1.e-6
5    21    0.3
21   21    0.3
5    5     0.3
21   5     0.3
```

Figure 76: Well parameter file required for runs in Example 1: Runs 1, 2, 3, and 4.

```
  50
  2.0    -200.00    0.00    0.00     0.00
  4.0    -200.00    0.00    0.00     0.00
  6.0    -200.00    0.00    0.00     0.00
  8.0    -200.00    0.00    0.00     0.00
                      .
                      .
                      .
 96.0    -200.00   -20.00  -20.00  -200.00
 98.0    -200.00   -20.00  -20.00  -200.00
100.0    -200.00   -20.00  -20.00  -200.00
```

Figure 77: Flow rate data required for runs in Example 1: Runs 1, 2, 3, and 4.

```
  4   50
  2.000  2955.301  1.0  3007.868  1.0  3007.991  1.0  3009.869  1.0
  4.000  2944.773  1.0  2999.921  1.0  3000.048  1.0  3002.754  1.0
  6.000  2936.084  1.0  2991.769  1.0  2991.896  1.0  2994.871  1.0
                      .
                      .
                      .
 96.000  2625.815  1.0  2678.215  1.0  2678.329  1.0  2625.813  1.0
 98.000  2609.079  1.0  2661.481  1.0  2661.595  1.0  2609.077  1.0
100.000  2592.349  1.0  2644.754  1.0  2644.867  1.0  2592.347  1.0
```

Figure 78: Observed pressure data required for runs in Example 1: Runs 1, 2, 3, and 4.

```
0 0 0 0 0 0 0 0 0 0 0 0 0 0 0 0 0 0 0 0 0 0 0 0 0 0 0 0 0 0 0 0 0 0 0
0 0
 .
 .
 .
0 0
0 0
0 0 0 0 0 0 0 0 0 0 0 0 0 0 0 0 0 0 0 0 0 0 0 0 0 0 0 0 0 0 0 0 0 0 0
0. 0. 0. 0. 0. 0. 0. 0. 0. 0. 0. 0. 0. 0. 0. 0. 0. 0. 0. 0. 0. 0. 0. 0. 0.
  0.   0.
    .
    .
    .
  0.   0.
0. 0. 0. 0. 0. 0. 0. 0. 0. 0. 0. 0. 0. 0. 0. 0. 0. 0. 0. 0. 0. 0. 0. 0. 0.
```

Figure 79: Boundary data required for runs in Example 1: Runs 1, 2, 3, and 4.

```
Initial Pressure file
1
Initial Pressure (PSIA)
 3014.70
 3014.70
 3014.70
    .
    .
    .
 3014.70
 3014.70
 3014.70
```

Figure 80: Initial pressure data required for runs in Example 1: Runs 1, 2, 3, and 4.

```
SGSIM Realizations
  2
phi
ln(k)
  .4000    3.1500
  .4000    3.1500
  .4000    3.1500
     .
     .
     .
  .4000    3.1500
  .4000    3.1500
  .4000    3.1500
```

Figure 81: Initial porosity and ln(k) field data required for runs in Example 1: Runs 1, 2, 3, and 4.

References

[1] C. V. Deutsch and A. G. Journel. *GSLIB: Geostatistical Software Library and User's Guide*. Oxford University Press, New York, 2nd edition, 1998.

[2] X. H. Wen, C. V. Deutsch, and A. S. Cullick. High-resolution reservoir models integrating multiple-well production data. *SPE J*, pages 344–355, December 1998.

[3] W. Xu, T. T. Tran, R. M. Srivastava, and A. G. Journel. Integrating seismic data in reservoir modeling: the collocated cokriging alternative. In *67th Annual Technical Conference and Exhibition*, pages 833–842, Washington, DC, October 1992. Society of Petroleum Engineers. SPE Paper Number 24742.